3. Instrument concept

IMAKA was conceived as a ground layer adaptive optics (GLAO) imager capable of delivering 0.3 arcsec or better images over a 1.0 degree diameter field for 150 nm wide spectral bands centered between 400 nm and 1000 nm. The goals of the technical parts of the Feasibility Study were to 1) define a general instrument concept, and 2) identify and explore technical issues which might be problematic in realizing a functional instrument.

The instrument concept for IMAKA, as it has evolved, will need either a dedicated upper end or full access to the volume behind the primary mirror cell and includes the following major components:

1. the CFHT telescope in something close to its current operational configuration
2. imaging optics which provide both a one degree diameter field with excellent IQ and an accessible, well defined image of the telescope pupil.
3. An adaptive mirror (DM) conjugate to a location close to the likely sources of ground layer turbulence – i.e not far from the telescope pupil.
4. DM control hardware and control computing facilities
5. A CCD camera system based on orthogonal transfer (OT) technology, together with standard b,g,r,i,z,and Y broadband filters.
6. An atmospheric dispersion corrector.
7. A set of approximately 6-8 wavefront sensors well distributed over the field
8. A CCD camera and DM location on the telescope at locations accessible for general maintenance.
9. A data reduction pipeline to provide astronomy-ready images with instrumental signatures removed.

For the feasibility study we concentrated on those issues which appear to be the most challenging, with the intent of leaving other, better understood issues, to Phase A engineering studies where technologies or current practices seem to be well defined, but where more detailed design decision will start to be made. We therefore left details of the ADC, DM and control, wavefront sensors and the data pipeline in this latter category.

3.1 Optical design:

The biggest challenge in the optical design was to determine, given the field size, whether or not a design was even feasible. The following top level instrument requirements flow from the IMAKA science cases and functional limitations imposed by the telescope:

Top-Level Instrument Requirements

1. Field of view : 1 degree diameter or equivalent solid angle
2. Wavelength Range : 0.4 – 1.1 micron
3. Delivered image quality of 0.3” or better at r band under median conditions, FWHM uniform within 10% over entire field
4. Photometric measurements with an accuracy of 1% absolute, 0.1% relatively
5. Astrometric measurements with an accuracy of 40mas absolute and 0.8 mas relative
6. Sky coverage 100% in Galactic plane and ≥ 50% at North Galactic Pole

Top-Level Functional Requirements

1. Wavefront sensors must sense the wavefront aberrations across the field that arise from effects near the ground.
2. The DM must correct this wavefront across the field.
3. Access to the CCD camera and DM systems should be provided with IMAKA on the telescope.
4. IMAKA should not preclude the use of other CFHT facility instruments
5. An exchange to IMAKA should be completed in less than one working day
6. IMAKA should be operational by 2016.

Given these requirements, the optical design is faced with the following challenges:

- Provide 0.15 arcsec (or better) images across a field 1 degree in diameter (or equivalent) for each spectral band (residual wavefront errors will then degrade IQ to 0.3 arcsec).
- Use an adaptive optical element that can be manufactured, working at an incident angle of less than 20 degrees and conjugate to a zone between 15 m below the primary mirror to 30 m above the primary mirror – required for effective GLAO correction across a one degree field
- Deliver a final f/5.7 beam – a requirement imposed by the desired image sampling of 0.1 arcsec per pixel for an orthogonal transfer CCD with 10 micron pixel pitch (later relaxed to include provision for an f/6.8 beam using a 12 micron pixel pitch).
- Provide a well defined pupil image and be able to locate a DM at that image.
- Locate optical and CCD camera components at accessible locations on the telescope
- If at the Cassegrain focus, pass the beam through the primary mirror's central hole.
- Use refractive materials (if any) that are available commercially at the required sizes.

IMAKA optical design requirements pose a serious design challenge. The needs for a large focal surface (~ 360 mm diameter), and for an adaptive element near a pupil image, require IMAKA to be physically large. A further consequence of the large focal surface is that in order to feed light to an array of wavefront sensors, which must span the one degree field, we will need to place pickoff mirrors very close to the final focal surface. As a result, the wavefront pickoffs may be located behind the bandpass filters. This places constraints on guide star flux and the associated available star counts. The wavefront sensor feeds will also vignette small areas of the focal surface.

Because of the difficulty inherent to the IMAKA optical design problem we engaged the services of 6 optical designers familiar with designing high performance optical systems for astronomical facilities and evaluated 17 or so design variants. Of these, only the two options presented here meet the core requirements of image quality, field size, pupil image quality, conjugation and focal surface access. These are discussed in the following sections. The remaining designs are briefly discussed in an appendix.

3.1.1 Prime Focus Design

The prime focus design by Clinton Evans and Hua Lin at COM DEV (Ottawa, Canada) splits the field into two rectangles measuring 0.4 degrees x 1.0 degree with centers separated by 2 degrees on

the sky. Two separate and independent optical systems together providing areal sky coverage equivalent to a one degree diameter, are mounted outboard of the telescope top ring. Image quality remains excellent if the fields are increased as much as 30% in the longer field dimension, at the expense of larger optics and detectors and provides potential regions for wavefront sensors near the field edges.

The all-reflective COM DEV design, one channel of which is shown below, uses 2 flat mirrors, 2 off-axis aspheres and a mildly convex spherical DM 260 mm in diameter. The aspheres are large - 65 cm and 90 cm respectively - which will make fabrication and testing expensive. The focal surface is curved (r = 1.6 m) but can accommodate flat 4k x 4k OT CCDs without serious IQ degradation if they are offset in focus in steps of 60 um.

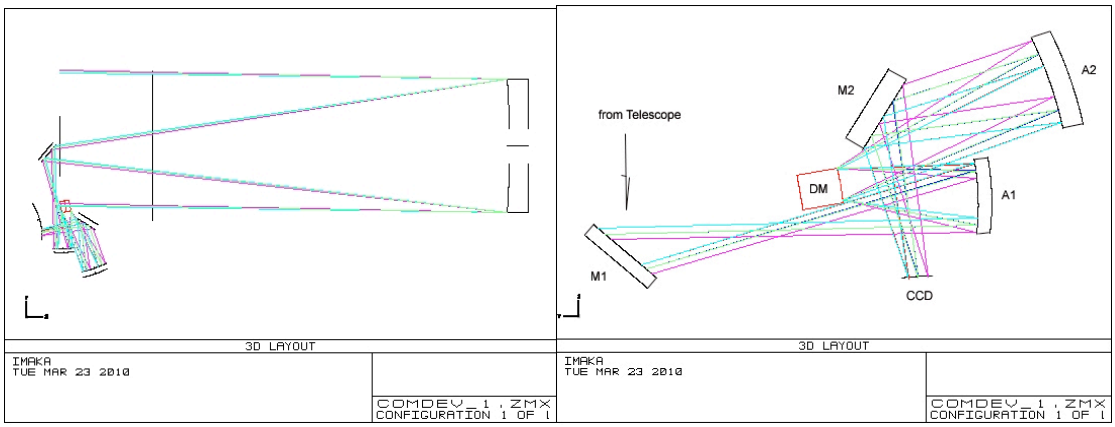

Figure 6: Layout of the COM DEV Prime focus design. Only one of the two sides is shown.

The physical units mounted to a dedicated upper end present some handling challenges since the current upper end handling ring will not pass over the cameras. However, the upper end could potentially be mounted first, with the separate instrument boxes attached afterward.

As laid out currently, each unit will vignette a small portion of the other's pupil and an even smaller portion of its own pupil, but the effects are small.

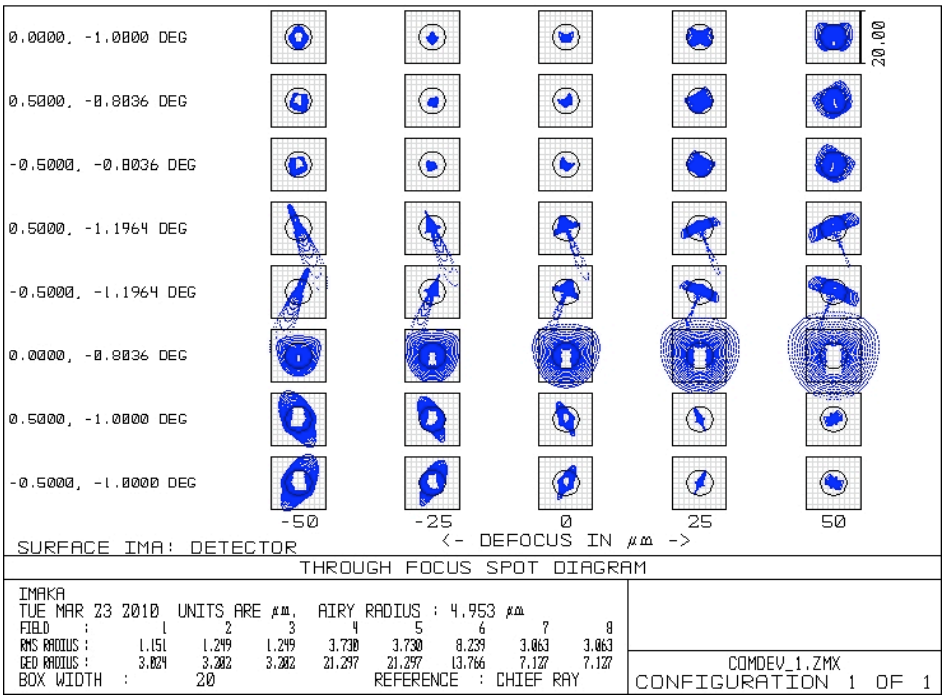

Figure 7: Performance of the COM DEV design. Spot diagram thru-focus

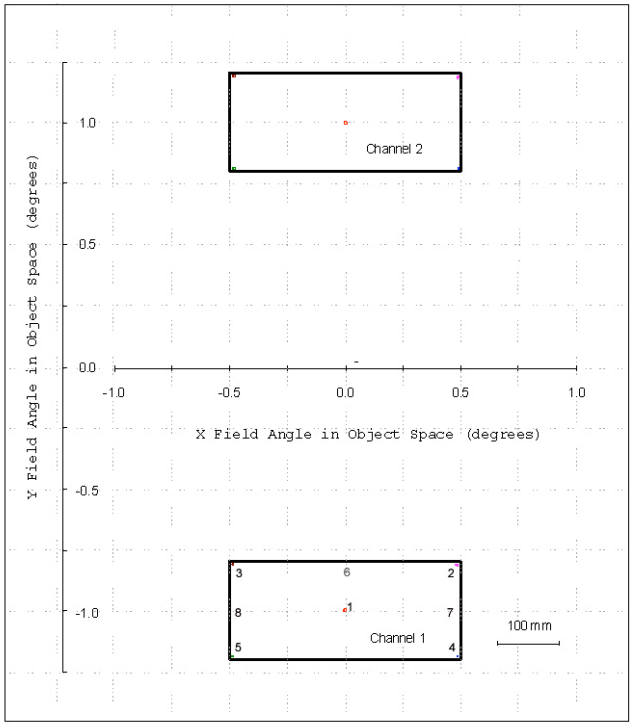

Figure 8: Science field layout of the COM DEV design.

Image quality is shown in the spot diagram above. Focus, in 25 um steps, runs from left to right.

Field position runs vertically. The locations of each row in the field are shown numerically in the lower diagram. Note that the worst images occur at the point closest to the telescope optics axis. Field extensions with good image quality to the right and left are possible.

Each spot diagram is contained in a 20 um x 20 um (2 pixel x 2 pixel or 0.2 arcsec x 0.2 arcsec) box. The circle in each shows the diameter of the first Airy diffraction ring for a wavelength of 0.7 um.

The footprint of the pupil on the DM is reasonably sharp. The maximum pupil aberration is 5.1% of the illuminated DM diameter. Each cluster of points in the diagram below indicates the ray intercepts for each of the extreme field angles. The DM is conjugate to a plane 7.8 m below the primary mirror.

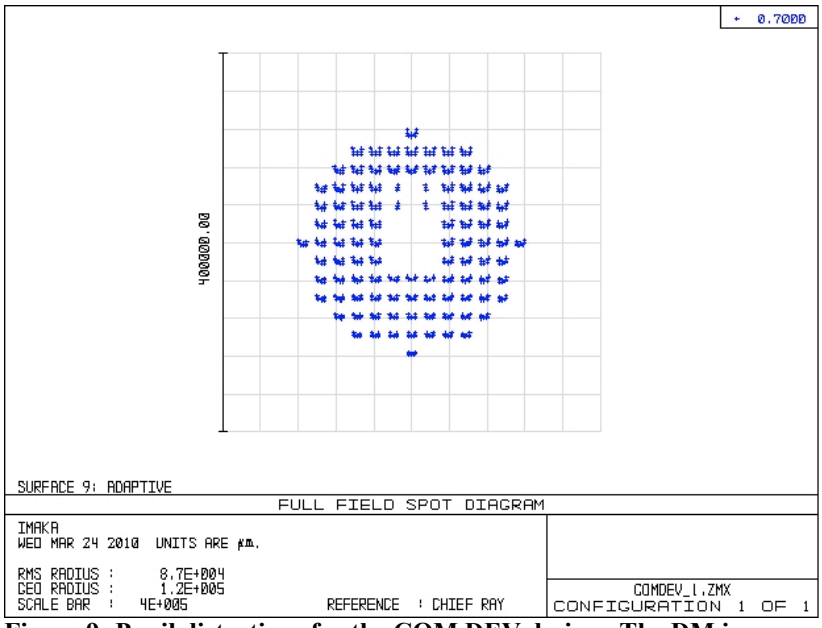

Figure 9: Pupil distortions for the COM DEV design. The DM is slightly misconjugated by about 8 meters.

This design's field geometry has a downside for objects with angular sizes between several degrees and 0.4 degrees, since mosaicing will be inefficient.

Computer-generated solid model drawings of an upper end incorporating the two channels of the COM DEV design, a cutaway showing the placement of the optics, and an illustration showing the system mounted on the telescope are provided below. The channels are shown mounted east-west, but could just as easily be oriented north-south.

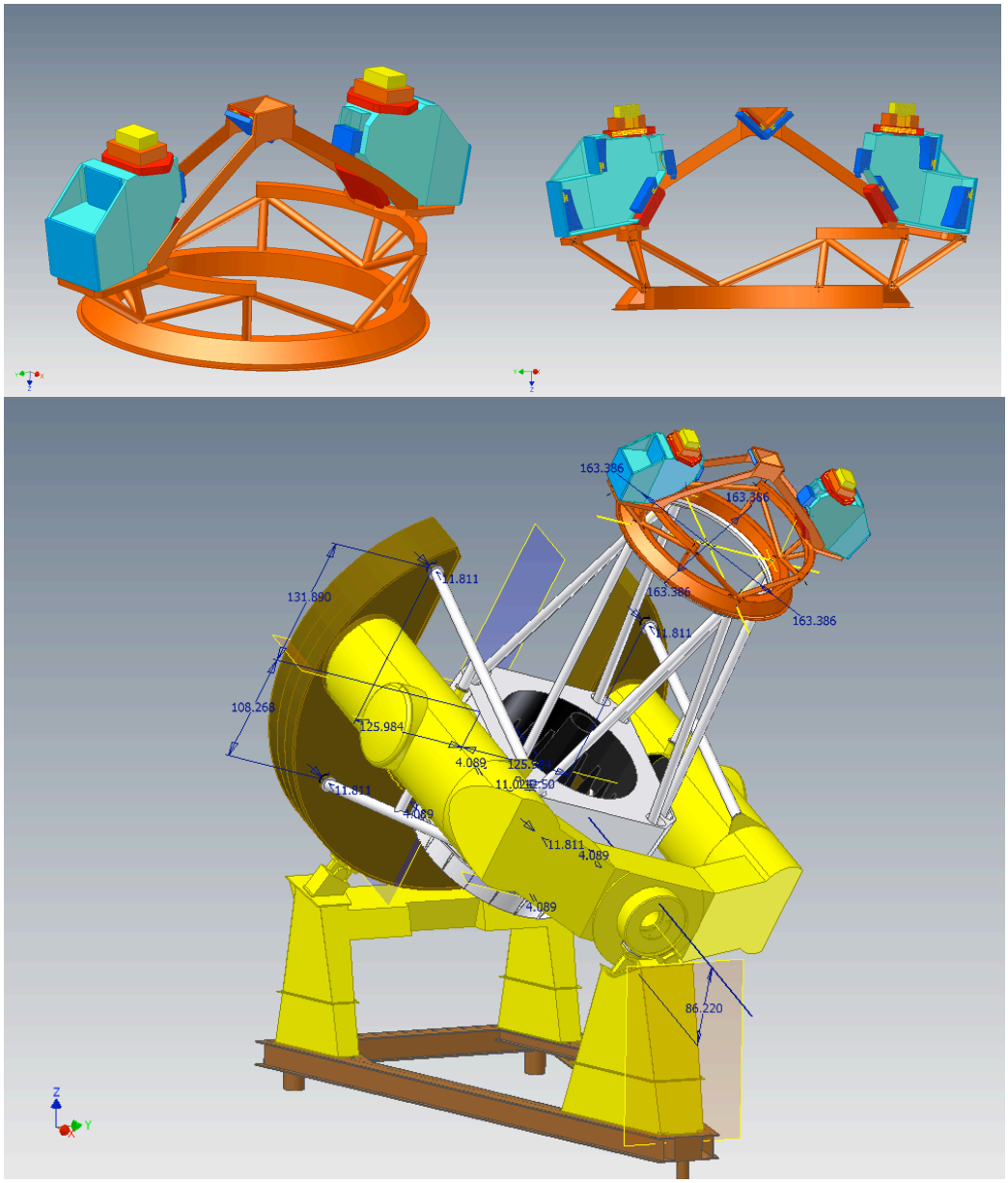

Figure 10: Mechanical layout of the COM DEV prime focus design

3.1.2 Cassegrain Design

John Pazder at HIA developed a potentially interesting double pass, Wynne-Dyson design for the Cassegrain focus with a contiguous, on-axis one degree diameter field. The design is rather unique since several lenses are used double pass with the entrance beam passing to one side of lens center while the exit (from the DM) beam passing through the opposite side of the lenses. This design has not benefited from the level of optimization evident in the COM DEV prime focus design, but still meets many of the design requirements. The design uses mostly refractive optics, except for the DM and a fold mirror. The 400 mm diameter DM has the advantage of being slightly concave which facilitates testing. There is ample room for an ADC, for filters and for wavefront sensors. The full one degree beam diameter (470 mm) passes through the primary mirror's central hole (680

mm) with ample clearance. Three lenses are mounted either inside the primary mirror cell or in the primary mirror's central hole.

The design's chief drawbacks are its very large size and thus its weight, several very large lenses, 22 air-glass interfaces without counting the ADC, filter or cryovessel window, a refigured secondary mirror, and the loss of the Cassegrain Bonnette which will need to be removed, probably on a permanent basis.

The large first diagonal mirror measures 54 cm x 76 cm, while the two large double-pass lenses measure 68 cm x 116 cm and 68 cm x 94 cm respectively. The secondary mirror sits at the same location as the current f/8 secondary mirror, but the figure needs to be changed to a longer radius and a stronger hyperbolic shape. The central obstruction defined by an upper Cassegrain baffle results in vignetting of roughly 19 % of the beam surface area much as the current f/8 system does, with a slight increase to 22 % at the edges of the one degree field due to vignetting at the undersized clear diameter of the secondary mirror.

The optical layout is shown in the diagrams below that include side and plan views.

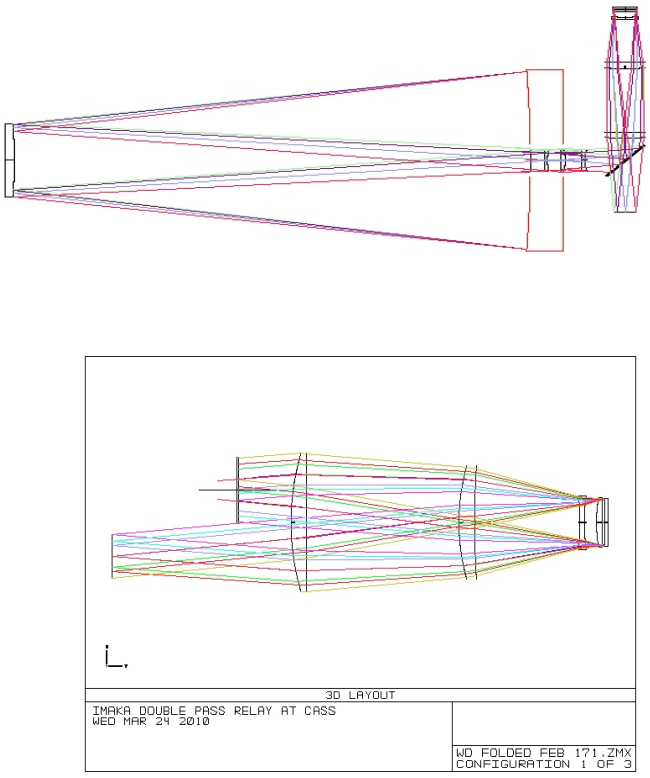

Figure 11: Optical layout of the Cassegrain Wynne-Dyson design

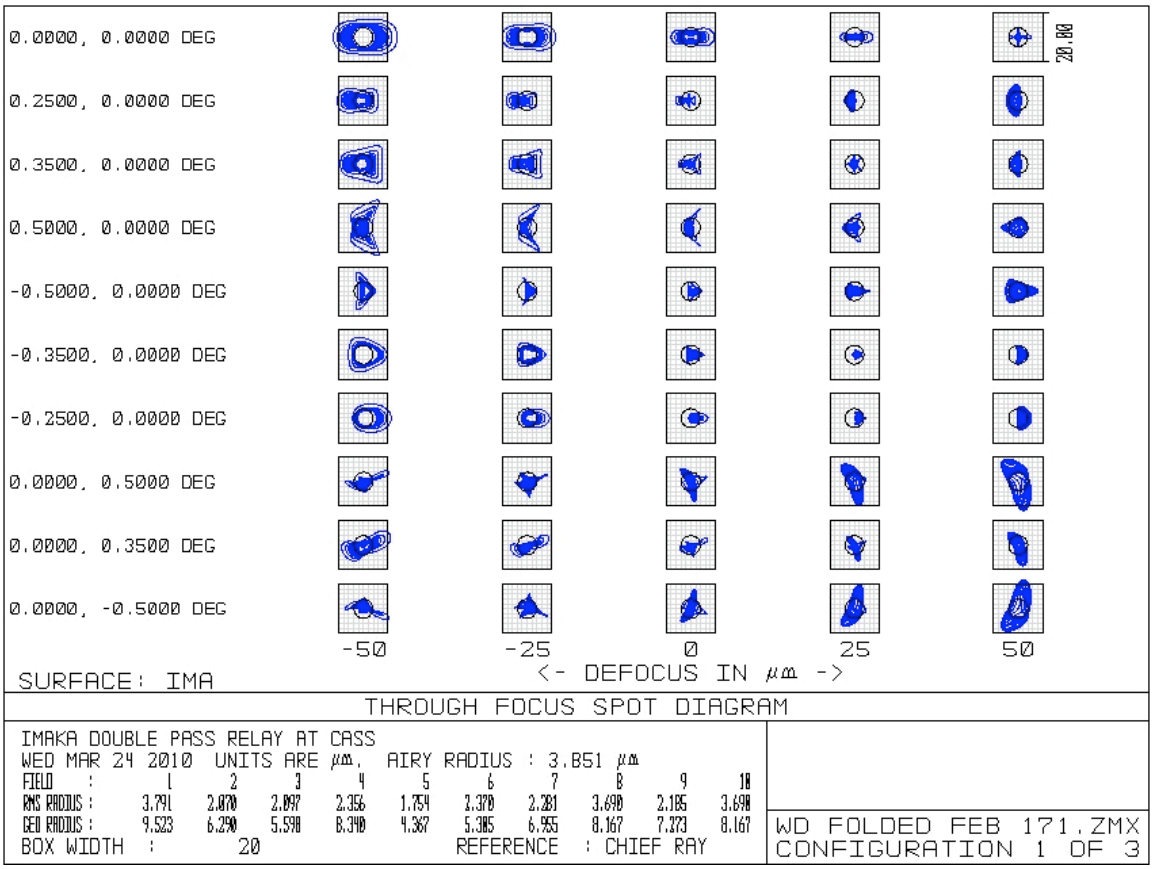

Figure 12: Performance of the Wynne-Dyson design: spot diagrams through focus

Image quality is shown in the spot diagram above. Focus, in 25 um steps, runs from left to right. Field position runs vertically and is listed on the left. Each spot diagram is contained in a 20 um x 20 um (2 pixel x 2 pixel or 0.2 arcsec x 0.2 arcsec) box. The circle in each shows the diameter of the first Airy diffraction ring for a wavelength of 0.7 um.

The footprint of the pupil on the DM is sharp. The maximum pupil aberration is 1.7% of the illuminated DM diameter. Each cluster of points in the diagram below indicates the ray intercepts for each of the extreme field angles. The DM is conjugate to the primary mirror.

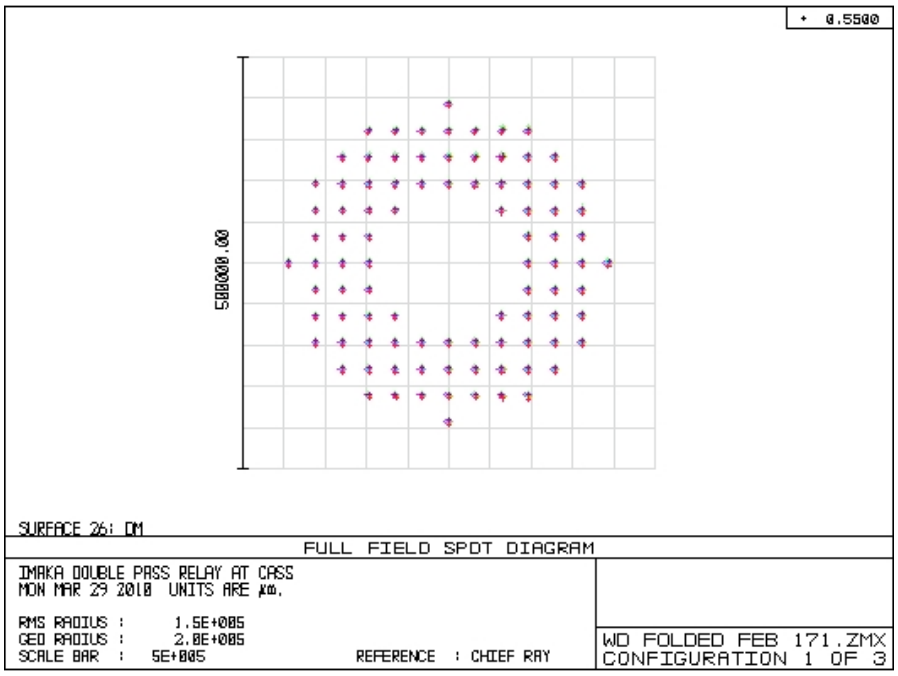

Figure 13: Wynne-Dyson design pupil distortions. DM is conjugate to pupil

The physical layout of the optics is shown below. Lenses L1 through L3 reside inside the primary mirror cell. The physical size of this configuration can be seen on the two images showing the optics on the telescope.

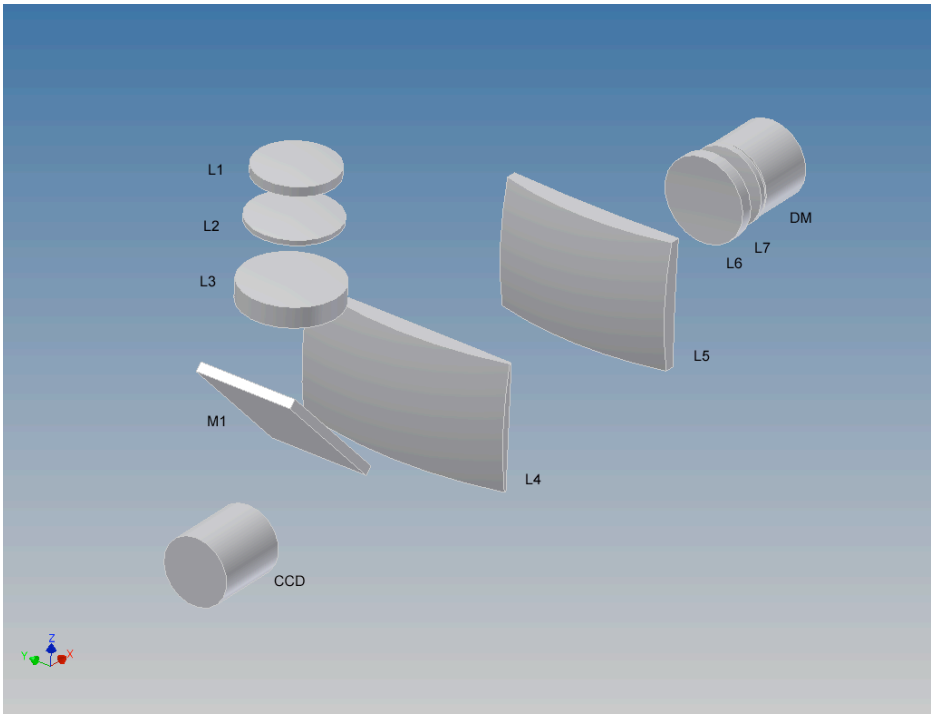

Figure 14: Optical layout at Cassegrain focus of Wynne-Dyson design

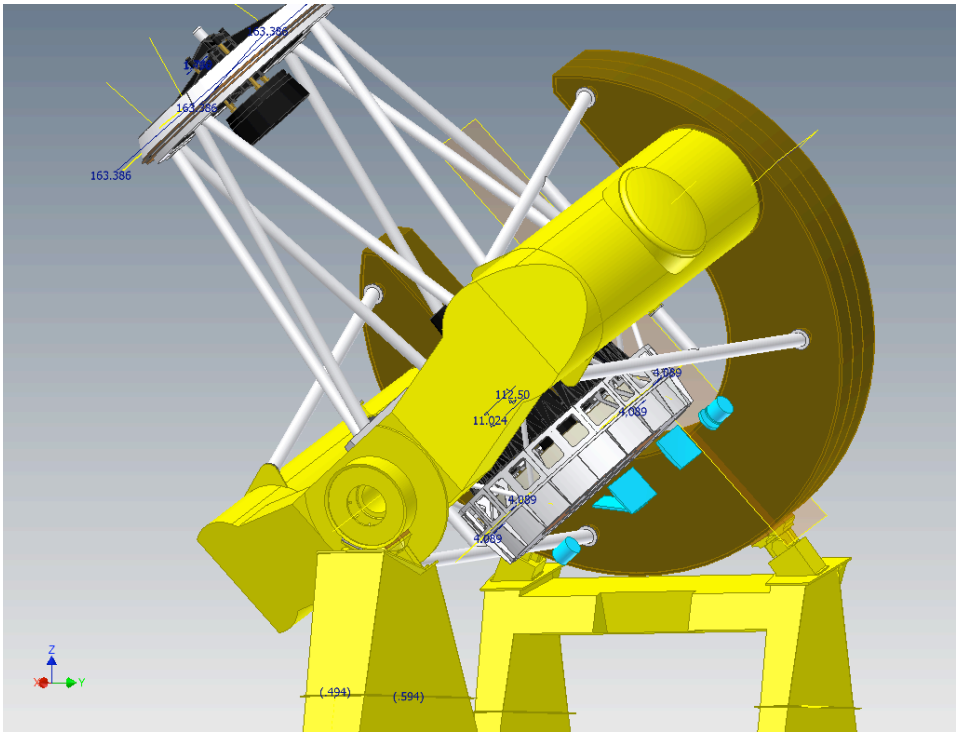

Figure 15: Mechanical layout of Wynne-Dyson design

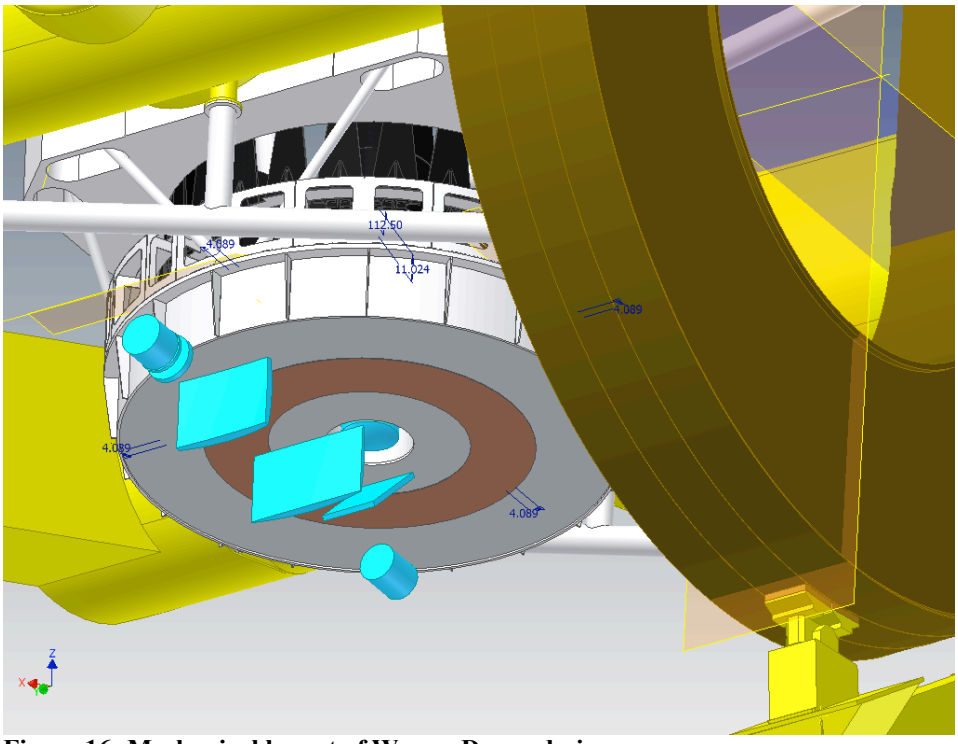

Figure 16: Mechanical layout of Wynne-Dyson design

3.1.3 Optical Design Technical Risks

3.1.3.1 Baffling

Baffling of a wide-field imager is critical to maintain low background sky levels. Stray light suppression and baffling design will need to be carefully considered during Phase A studies, especially for the prime focus design where it will be particularly important to ensure that the detector sees only the beam as it leaves each of the upstream optical surfaces. Otherwise, light from the moonlit sky and nearby bright stars could lead to unacceptable background levels and focal plane artifacts. Both designs, however, offer potential locations for baffles.

3.1.3.2 Glass availability

Glass availability for IMAKA is a concern given the large sizes. Optical glass availability becomes problematic for some glass with blank sizes larger than 300mm diameter, and virtually all glasses for diameters larger than 1000mm. For some glasses crystallization during casting and cooling is a problem; these are Lathanum (LAK,LAF and LASF), phosphate (PSK, PK) and fluorine (FK) glasses. For these glasses Schott's current production limits are 300mm to 360mm diameter. For other glasses, the size limit is simply the casting time to pour such a large blank limits the size limit. Annealing is also a consideration, as the time to anneal also goes up significantly with blank size. For meter size optics this is measured in month, pushing the price up. Schott information circular "TIE-41 Large Optical Blanks" gives considerable information on optical blanks and is worth reading. Table 1 from that report gives a summary of availability and is reproduced below.

Glass Type Family	Melting Technology Min Prod*	Max Dim present capabilities	Max Dim with development	Restricted by	Preferred Glass Types
BK	Cont. Tank 5 tons	∅1000 x 300	∅1500 x 500 or equiv. Vol	CT, CS, ES	N-BK7
LLF, LF, F, SF	Cont. Tank 5 tons	∅1000 x 300	∅1500 x 500 or equiv. Vol	CT, CS, ES	LLF1, LF5, F2, SF6
FK, PK	Discont. Pot	∅360 x 60	∅460 x 100	Cryst, VS	N-FK51A
LAK, LAF, LASF	Discont. Pot	300 x 160 x 43 GD	360 x 280 x 80 GD	Cryst, VS	LAK8, LAK9
KZFS	Discont. Pot	300 x 160 x 43 GD	360 x 280 x 80 GD	Cryst, VS	KZFSN4

Table 1: Glass types and their associated production information

Min Prod*	Minimum production amount needed for high quality
CT:	Casting Time
CS:	Center-
ES:	Edge-
VS:	Volume Striae
Cryst:	Crystallization
GD:	Gross diameter

Table 7: Schott "TIE-41 Large Optical Blanks" summary of availability

3.1.3.3 Procurement of large optics

The main challenges for the COM DEV prime focus design will be the pair of off-axis aspheres and

the two large flats. The flat in the primary mirror beam measures roughly 600 mm x 600 mm, while the fold flat located just before focus is approximately 600 mm x 740 mm. These are not unduly large and should be readily fabricated.

The two aspheres, which measure 550 mm x 650 mm and 700 mm x 900 mm respectively, will be more of a challenge. The test configuration for these will likely be as expensive as their fabrication. Several material choices exist. Diamond turned metal mirrors are enticing since standard technologies exist for their fabrication and mounting hardware can be configured directly as part of the optic. The challenges will be to produce a surface of sufficient accuracy and smoothness needed for work at the shorter wavelengths, and to maintain the optical figure in an environment with changing environmental temperatures. Options for coating and recoating the optics will be a consideration.

In all four cases weight will need to be considered, so more exotic material such as beryllium or tungsten carbide can be considered, although each comes with its own issues. On the more conventional side, monolithic or light weight glass substrates are attractive options..

However, no matter the material of choice, the technologies exist for mirror fabrication. Housing and mounting too will have their challenges, but again, these seem tractable.

For the Cassegrain Wynne-Dyson design the biggest challenge will be obtaining glass blanks for the two large lenses. These measure 680 mm x 1160 mm and 680 mm x 940 mm respectively. The materials, BK-7 and SF-6 are among the most common optical glasses and are available in large sizes. Detailed discussions will be needed with glass vendors to ensure that glass of the required index uniformity can be provided although initial discussions by the designer suggest that suitable optical blanks should be able to be realized. Lens mounting and self weight will be important considerations since obviously lenses cannot be light-weighted. As with the Prime Focus design, the flat mirror is large but its production should not present a ny undue challenges.

3.2 GLAO System and Components

As will be presented in the simulation section, the envisioned GLAO system has a correction order of ~20x20 actuators with 6-8 natural-guide star wavefront sensors on probe arms that acquire stars within the science field of view. Most of the components for the system are comparable to those in existing systems. The large field of view and relatively low temporal bandwidth required affords a nearly complete sky coverage with the GLAO system using available WFS detectors. The deformable mirror is comparable to existing DMs and the wavefront reconstruction hardware must handle a reconstruction on par with (and at slower speed) than many adaptive optics systems that are being built. The principle engineering challenge will be the acquisition and positioning of the multiple wavefront sensors.

3.2.1 Adaptive (Deformable) Mirrors (DM)

Deformable mirror technology suitable for ‘IMAKA exist now. Examples of DM systems delivered by CILAS (Orleans, France) to observatories are shown below. The size of these DM’s (for example 188 mm diameter for the system delivered to ESO shown on the right) compares favorably with the size required by ‘IMAKA which, for comparison, will requires a 20 x 20 square stacked-array DM with 330 actuators and 4 um actuator stoke.

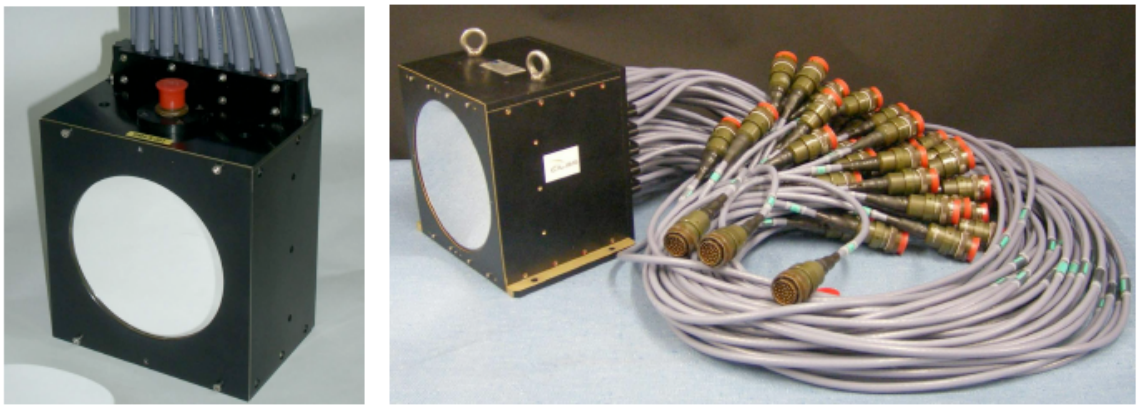

	SAM 52	SAM 185 (NAOS)	SAM 416 (Gemini DM4.5)	SAM 1377 (ESO-HODMAO)	SAM 4300 (TMT)
Max stroke (µm)	10	9,6	8,8	10	11,8
Individual Stroke (µm)	5	4	3,2	4	5,2
Interactuator Stroke (µm)	3	3	2,4	3	4,1
Matrix dimension	8	15	22	41	73
Number of actuators	52	185	416	1377	4200
Actuator spacing (mm)	8	8	5	4,5	5
Optical Aperture (mm)	80	112	106	180	360

Some Customers: ESO TMT, GEMINI, NSO, IAC, LAOG.

Figure 17: Examples of CILAS stack-actuator deformable mirrors and their performance specifications.

Technical details for some of these CILAS mirrors are listed above. The two optical designs we are considering for IMAKA each require a DM with a curved substrate. Recent enquiries with CILAS indicate that development of the specific DM's required by the IMAKA optical designs should not be a problem as indicated in the following note from Jean-Jacques Roland, the CILAS manager responsible for DM development.

> *"During the recent period we have start some work on large size, and spherical SAM DMs, not so far from your requirements. Jean-Christophe Sinquin, our technical manager will tell you more on the subject.*
>
> *We can propose to send you an answer with some technical comments, a ROM cost for each DM and a basic schedule during week 16 (between april 19 an 23)."*

3.2.2 DM drive hardware and computing requirements

The control hardware for the DM, including high voltage power supplies, cabling, high voltage drive amplifiers, fast D/A converters and computing facilities capable of real-time computations needed for DM control have all been realized on similar AO systems already or soon to be in operation. For example, the Keck AO systems, commissioned more than a decade ago, are based on DMs with 349 actuators and run at kHz rates. Due to the low-speed wavefront deformations associated with ground layer and in-dome turbulence, IMAKA will operate at a lower bandwidths.

This should lower the computational bandwidth requirements for the GLAO system proportionally.

3.2.3 Wavefront Sensors and Detectors

The wavefront sensor cameras themselves do not depend on any development. Existing CCDs already have sufficiently low read noise levels (e.g. 3 electrons read noise) that are suitable for the `IMAKA WFSs.

The challenge will be to engineer the mechanisms to position the wavefront sensor probe arms within the field of view. We acknowledge that we have neglected the conceptual design of this element. We believe it is a challenging technical hurdle but one that does not present any fundamental limitations to the approach and which can only be addressed in earnest within an overall opto-mechanical design. We also note that the equatorial mount of the telescope will greatly simplify these mechanisms since the sky orientation is fixed as the telescope tracks across the sky.

3.3 The Camera

The `IMAKA OTCCD camera has not been identified as a critical element requiring a special focus during this extended feasibility study because such systems have been built and put in operation on the sky by members of this current study. They are however still in the process of perfecting the technology and this report presents a short summary of its current state.

3.3.1 OTCCD cameras

There are currently two major projects using/developing large OTCCD cameras: the GigaPixel Cameras 1&2 (GPC1, GPC2) for use on the PanSTARRS 1&2 (PS1, PS2) telescopes atop Haleakala led by the PanSTARRS consortium, and the One Degree Imager (ODI) on the WIYN telescope at Kitt Peak (WIYN consortium). All three cameras use a similar square shaped mosaic of i) 60 (on a 8x8 footprint) OTCCDs for GPC1/2 and ii) 64 (8x8) for the ODI. Each OTCCD is a monolithic area of 64 (8x8) OTCCD cells of 600x600 pixels each. In total, there are approximately 38 kpixels across the focal plane making them 1.4 Gpixels cameras. The PanSTARRS camera has a pixel scale of 0.26 arcsecond (sampling a 0.9" seeing) and covers 7 square degrees. ODI has a pixel scale of 0.1 arcsecond (sampling a 0.55" median seeing after OTCCD correction) and covers 1 square degree.

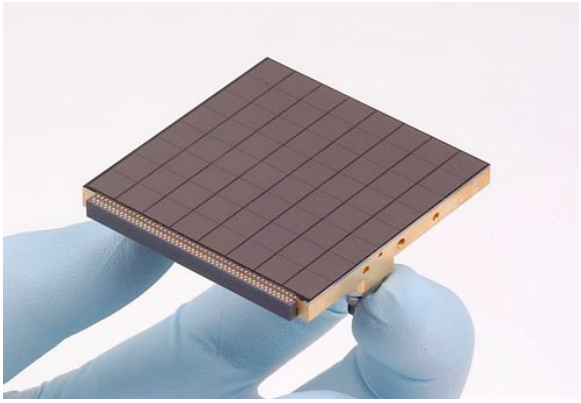

Figure 18: One of the 60 Orthogonal Transfer Array (OTA) devices that is used in the Pan-STARRS gigapixel camera. The OTA (shown here in its front-illuminated version) consists of an 8 x 8 array of 600 x 600 CCD devices, each of which can be controlled and read out independently.

PanSTARRS GPC1 and GPC2

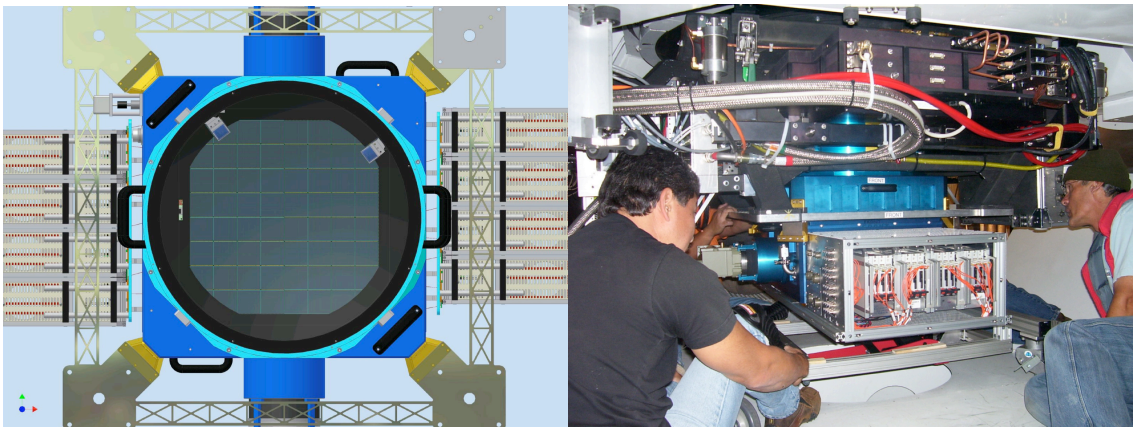

Figure 19: Pan-STARRS 1 GPC1: (Left) Upper view schematic of the Pan-STARRS gigapixel camera (Right) The first gigapixel camera installed at the focus of the Pan-STARRS 1 telescope.

GPC1 has been on the sky in operations for almost three years, and while various performances have been tweaked (lower read noise, currently around 6 electrons, glowing on the Lot 1 MIT/LL devices), the OTCCD function so critical to `IMAKA has not yet been investigated due to other higher priority issues for the project. The predominant on-going challenge has been tracked to a poorly designed secondary support which caused the collimation of the telescope (and hence the PSF) to be very unstable, a problem which has now been addressed and GPC1 on PS1 is in science operations since early 2010. There are still residual issues on the image quality delivered by the telescope and the OTCCD correction will not bring any tangible improvement to the PSF until this issue is addressed. Although it is expected that GPC1 will eventually use OTCCD correction, its main science goals are achievable with only telescope guiding (median image quality currently at 1.0"). This will be the first mode of OTCCD correction they will implement.

It is worth noting that after the OTCCD was invented by John Tonry et al. in 1997, many scientific articles have been published using data obtained with OTCCD correction from the OPTIC camera (a 16 Mpix OTCCD camera) mounted on the UH 2.2m telescope atop Mauna Kea, including key topics on precise photometry. This camera is also loaned on a regular basis to the WIYN telescope. Based on the encouraging results on image quality improvements, WIYN decided to invest in this technology on an instrument of their own, the One Degree Imager (ODI).

WIYN ODI

WIYN developed a prototype of the ODI, QUOTA (Quad Orthogonal Transfer Array) to qualify the technology on a larger scale, especially to test and qualify the new detectors planned for the ODI. Unlike GPC1 which makes use of the MIT/LL detectors, QUOTA and ODI use DALSA devices, which have a similar layout as the MIT/LL OTCCD (DALSA licensed the design from MIT/LL) but different pixel size. It is worth noting that having two major CCD players such as MIT/LL and DALSA investing time and energy in the OT technology will benefit the astronomical community on the long term. QUOTA was put on the sky as a technology qualification and has not been offered for scientific use (it was made of two frontside illuminated devices, and two backside illuminated devices) and indeed the PSF was substantially improved within several arcminutes of

the guide star (within the isokinetic angle). OPTIC remains available to the WIYN users while the development of the ODI relies now on devices procurement from DALSA and thinning by Mike Lesser. The current delivery date has been pushed to mid-2011 due to manufacturing issues at the foundry, hence first light of the ODI is not expected before the end of 2011 at the earliest.

3.3.2 Devices & procurement

The GPC1/GPC2 use devices from MIT Lincoln Lab, the laboratory at the origin of the very first OTCCD back in the late 90s. The conclusive results motivated the grand scale approach from the Pan-STARRS project. GPC1 uses Phase 1 MIT/LL devices on the PS1 telescope and Phase 2 MIT/LL devices are being fabricated in early 2010 for the GPC2 on PS2, the second Pan-STARRS telescope. Here is the list of various lessons learned over the course of the OTCCD and PS1/PS2 development ranked in order of importance. Some of these issues have already been addressed, some are still being investigated (Barry Burke, MIT/LL, 2009/2010, private communication):

1. **Read Noise**: The GPC1 achieves 6 to 7 electrons noise (the median noise among the 3840 amplifiers is about 6.3 electrons). This is above the target of 5 electrons per pixel. MIT/LL studied the problem and made some modifications to the output circuitry which are currently being tried on the new Pan-STARRS devices. Final noise performance will be established by this summer. A different output design (pJFET) was tried on some recent Pan-STARRS development devices, and from limited testing did achieve less 5 electrons read noise. However, that amplifier has a higher conversion gain and becomes somewhat nonlinear at levels above 50,000 electrons. MIT/LL is hoping to put some effort into fixing that issue. A low read noise is of great importance for `IMAKA as the pixel scale of 0.1"/pixel will lead to limited sky level counts, while the full well is also key to achieve a high dynamic range.

2. **Packaging**: There are flatness issues with the GPC1 devices packages which employed a relatively thin piece of molybdenum. The difference in coefficients of thermal expansion causes the devices to dome upward when cold. For GPC1 this non-flatness was addressed by dishing the molybdenum prior to packaging, but GPC2 will have a completely different package, based on silicon attached to an aluminum nitride circuit that has been lapped flat at the 1 micron level. All in all, 10 microns peak-valley is a realistic goal for the final devices. This will meet the specification for depth of field on `IMAKA.

3. **Device thickness, quantum efficiency and fringing**: The current devices are 75 microns thick and there are plans to go to 125 microns for improved red response and further reduced fringing in the red. The current devices exhibit a 2% peak-valley fringe amplitude in the Y band, and show virtually no fringing in the z' and i' bands. This should be compared to the 15% fringing in the z' for MegaCam which limits its scientific capabilities at those wavelengths. At 2% (or less for the 125 microns devices), the data processing of OTCCDed data should not be an issue, especially since the scale appears to be much larger (10 arcsec.) than the expected pixel shifts (less than 1 arcsec.). A quantum efficiency of 30% at 1 micron is currently achieved by the Lot 1 devices, and would be further improved with a 125 microns thickness. The following graph shows two quantum efficiency curves: the red curve is from a Pan-STARRS device with a coating optimized for minimal fringing in the near IR. The blue curve is from a 36 microns thick CCD with a new coating (measurements by Chris Stubbs' group at Harvard). The gain in the blue response is of course at the expense of the near-IR because it is a thinner device. Further investigations are currently taking place to qualify this coating on devices of various thicknesses. `IMAKA's best angular-resolution being in the red

part of the spectrum, it seems logical to favor a thicker device: the average quantum efficiency over the Y band for this 75 microns thick device is 40%!

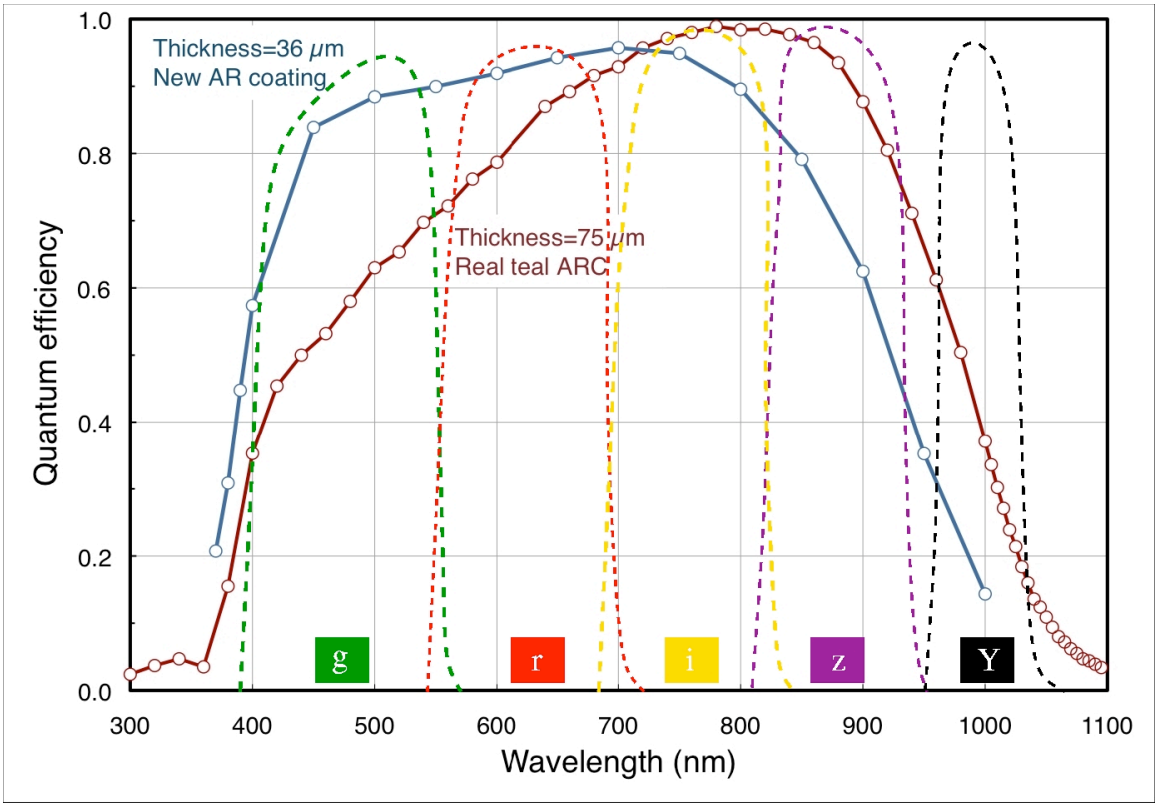

Figure 20: PanSTARRS1 GPC1 detector efficiencies and filter transmission curves.

6. **Well capacity**: GPC1 devices have only about 50,000 electrons well capacity (80% of the focal plane), but a recent redesign led to more than 75,000 e-. Going to larger pixels (12 microns instead of the current 10 microns) would help obviously. See the discussion on read noise above for a note on `IMAKA's dynamic range.

7. **Logic and amplifier glow**: Changes were made to the transistor layouts which resolved these issues caused by having nMOS logic sitting next to a very sensitive CCD. There is a development underway to make an OTCCD without the logic, which should be ready in time for `IMAKA.

7. **Fill factor**: The fill factor defines how effective similar detectors can be assembled together in a packed focal plane to minimize dead spaces. The GPC1 devices have a detector fill factor of 90%. The new devices will reach 92%, comparable to MegaCam's 93% fill factor.

3.3.3 Acquisition chain

It is worth mentioning that WIYN adopted the detector controller developed by the Pan STARRS camera group (STARGRAP), a now well proven robust and reliable design (low read noise, fast readout). The entire focal plane is readout in 6 seconds (a gain in nearly an order of magnitude over MegaCam). The entire acquisition chain for this camera has been fully optimized for PS1 and matches well the requirements set for `IMAKA. We do not foresee needing further developments in this field for the `IMAKA project.

3.4 Operations and Data Processing

Here we present a brief discussion on the overall operations and data handling of an instrument like `IMAKA by CFHT. Specific operational modes and scenarios are left to a Phase A study but at this point we address the questions of whether there are aspects of the operation or data handling of the IMAKA instrument that present significant impasses to obtaining science quality data.

3.4.1 Operational Concepts

CFHT's observing environment

Today, CFHT provides exclusively service observing for its three main instruments: MegaCam, WIRCAM, and ESPaDOnS. As an imager, `IMAKA lends itself naturally to queue operation in this operational model. Importantly, the CFHT queue can already accommodate scientific requirements based on the delivered image quality and the addition of the Mauna Kea MASS/DIMM (MKAM) provides the real-time monitoring of the atmosphere to efficiently schedule `IMAKA. Queue observing will be a key operational element of `IMAKA to take full advantage of the delivered image quality.

The following paragraphs describe evolutions needed in the CFHT environment to accommodate this new instrument. The MegaCam observing environment encompasses the Queued Service Observing (QSO), the instrument control (NEO), the data processing pipeline Elixir, and the Data Archiving and Distribution System (DADS).

Queued Service Observing (QSO)

There will be three possible modes of operation of `IMAKA made available to the user based on the scientific requirements and the availability of guide and tip-tilt stars in the field:

- GLAO and full/partial OTCCD correction (expected as the dominant mode)
- GLAO and only global tip-tilt OTCCD correction
- No GLAO correction, but global tilt OTCCD correction (MegaCam mode)

Compared to MegaCam, the only evolution needed in the the QSO interface allowing the users to enter their observations (Phase 2 Tool, PH2) will be the inclusion of an automated interface defining how given sky regions will provide enough bright stars for GL correction (a handful is needed) and/or OT correction for the local tip-tilt OTCCD correction across the field of view (up to 200 stars can be needed over one square degree for optimal OTCCD correction).

New Environment for Observing (NEO)

The entire instrument must comply with the CFHT NEO interfaces. The PanSTARRS project adopted the MegaCam NEO interfaces (namely, software agents operating within the "director" environment) in 2006 for its first GPC1 camera. That camera is very similar to the one planned for use in `IMAKA so we expect that this system can be (re)adapted to CFHT.

The GLAO system comprises the adaptive optics control and the wavefront sensing, two entirely

new blocks. Their operations and calibrations will need to be developed and worked into the NEO environment. We expect that there will be subtleties in the acquisition and calibration of the GLAO and OTCCD systems. For example, during acquisition of the GLAO guide stars, stellar catalog position errors, mechanical flexure, and misalignment in the individual wavefront sensors will need to be compensated by active control servos that automatically position WFSs with their respective guide stars. While we expect that these controls are less sensitive than for systems like MCAO, where variations of things such as the focal plane plate scale are possible, further study is needed to detail the algorithms to automate the systems. We expect that the greatest effort will be to ensure that the acquisition process is smooth and efficient.

The development of the software for MegaPrime/MegaCam within NEO has proven that this environment and model of development is well tuned for very large scales instrumental projects.

Data Archiving and Distribution System

An `IMAKA FITS file will be very similar to a MegaCam file (Multi-FITS Extension, MEF) and no fundamental change in DADS is expected except for the handling of some new FITS keywords (e.g. interface with the GLAO and OTCCD controllers, etc.)

3.4.2 Data Processing

Detrending

The Elixir wide-field optical data processing pipeline has transitioned over two generations of CFHT wide-field optical imagers: CFH12K from 2000 to 2003, and MegaCam up to today.

The operation mode of `IMAKA will be very similar to these two instruments: observing runs of several weeks alternating with other instruments depending on the community pressure. The granularity of an observing run is expected to remain at least two weeks like MegaCam. As a consequence, the handling of data to produce master detrending frames by Elixir still applies unlike PanSTARRS1 which operates its camera continuously, calling for a different detrending strategy and overall pipeline architecture - the Pan-STARSS Image Processing Pipeline (IPP). While no change is needed in the current Elixir operational model, the detrending recipes will most certainly require extensive work to handle the specifics of OTCCD data (much is already being learned on these aspects as part of the PS1 IPP effort).

Due to fundamental differences in the scientific use of the instruments and the crucial need to reach a photon noise regime from the sky background per pixel, the data rate for `IMAKA will, in general, be lower than that of Pan-STARRS'. Pan-STARRS currently handles smoothly with IPP a flow of up 1.8 terabytes of data for a good night, with a median exposure time of 30 seconds (with an added 14 seconds for overheads, including the 6 seconds camera readout time). Due to the small projected area of the `IMAKA pixel (0.01 arcsec^2) on the sky, the photon regime will be reached 3.5 times slower than on MegaCam. Assuming a 5 electrons read noise, this means 9 minutes in the g band, 7 minutes in the r band, and 3 minutes for the i band. Over these three filters, the average exposure time is 6 minutes and leads to a data rate one order of magnitude lower than what is currently handled routinely by Pan-STARRS' IPP. Considering the constant evolution of computing and storage capabilities, we do not expect that `IMAKA data will represent a challenge in volume or in rate.

Looked at on pixel scales, OTCCDs call for a standard data processing, except in the red part of the spectrum where the fringe correction is complicated by the fact that the interference pattern, a static function of the geometry of the detector (thickness), will get smeared by the OT function. Since fringes variations with time are basically unpredictable, the best way to collect quality data in the z and Y band is to use high resistivity substrate devices generating very low fringing, such as the PanSTARRS OTCCDs manufactured by MIT/LL.

Photometric calibration

Photometric accuracy was a major technical challenge encountered on MegaCam by the Supernovae Legacy Survey (SNLS) with systematic errors limiting the Cosmology. Large efforts (Regnault et al. 2009) were produced by the SNLS team and CFHT to tackle these systematics and indicate that high quality photometry over a large field of view can be achieved: a 1% absolute calibration to the Landolt system is now achieved from the g to the i band.

To fully unlock the scientific potential of the SNLS, the entire photometric calibration must be brought into the Sloan system where better than a percent absolute photometric accuracy in all bands is expected. This overall effort is believed to be an important legacy for the next generation of wide-field imagers being put in operation throughout the world. The groups that led this effort are part of the `IMAKA science team, guaranteeing a passing of the expertise to the new instrument.

These techniques apply naturally to OTCCDs which have proven to achieve photometric precision equally good to standard CCDs (Tonry et al. 2008). An interesting experiment conducted by Howell et al. (2003) achieved ultra precise photometry with an OTCCD, down to a fraction of a milli-magnitude, proving in particular that this special pixel architecture and mode of operation does not affect photo-charge collection and preservation.

Astrometric calibration

The OT function removes the internal "elasticity" within the wide-field image, an elasticity experienced on MegaCam images throughout the field of view for example and blurred out only through long exposures. Along with the stable PSF, this elasticity removal should simplify the global astrometry. Dithered exposures made through several filters are however still a requirement to reach a precision of a few milliarcseconds with current reference catalogs. Elixir derives the MegaCam astrometry on a chip basis to within one arcsecond, leaving the field open for advanced softwares such as the SCAMP (Bertin 2006) to tackle very effectively precise astrometry at the scale of the whole focal plane. Mean RMS external of 45 milliarcseconds with respect to SDSS-R6 and mean RMS internal error of 4 milliarcseconds are currently achieved at Terapix on CFHTLS data. The SDSS astrometric catalog does not cover the entire sky but the GAIA mission ought to resolve that issue by 2015.

PSF modeling

Providing a model of the PSF in every point of the Imaka field at the level of accuracy required from some science drivers (e.g. weak lensing), is more challenging than for traditional ground-based wide-field instruments. Software such as PSFEx (Bertin 2010, in preparation) is already able

to model PSFs such as those expected from `IMAKA. But not unexpectedly, preliminary work conducted on `IMAKA simulations shows that the current generic polynomial model in PSFEx is unable to cope with PSF variations if PSF-fitting residuals on pixel scales are to be kept below a few percent. We plan to replace the polynomial variation model with more specific ones centered adaptively on the OTCCD guiding stars (ideally one per 4 by 4 square arcminutes). Stacks of dithered exposures will benefit from a PSF-homogenization process such as the one developed for the Dark Energy Survey (e.g. Darnell et al. 2009) or from a more sophisticated "image fusion" approach using e.g. Bayesian inference.

4. Optical Turbulence at CFHT

4.1 Introduction

The `IMAKA concept works because the delivered image quality is degraded largely by optical turbulence within a volume close to the telescope and/or ground. The CFHT MegaCam image quality study (Salmon et al 2009, PASP) and the Gemini ground-layer study (Chun et al 2009, MNRAS, 394) show that this is indeed the case for CFHT on Mauna Kea. Salmon et al. (2009) deduce the relative contributions to the delivered image quality of MegaCam images from a variety of sources (See below Table 4 from Salmon et al 2009). They find that the largest local degradations come from dome seeing (0.43" at 0.5 microns) and the telescope static optical aberrations (0.33" at 0.5 microns). Using an optical turbulence profiler, Chun et al. (2009) found that the atmosphere above the summit of Mauna Kea has a very thin, 30-50 meter thick layer of optical turbulence just above the ground and no other optical turbulence within the boundary layer (h<1km). Finally, multiple studies (Chun et al 2009, Schoeck 2010) have found that the free-atmosphere seeing above Mauna Kea is excellent (0.35-0.4" FWHM at 0.5 microns). These results suggest that GLAO on CFHT will provide a significant improvement to the delivered image quality of the facility over a very wide field of view.

Table 8: CFHT image quality error budget reproduced from Salmon et al (2009)

TABLE 4 (Salmon et al 2009) CONTRIBUTIONS TO MEDIAN IQ

(FWHM [″], 500 NM, ZENITH)

Individual Components and Values		Total (arcsec)
Atmosphere	General (0.49″) Ground layer (0.20″)	0.55″
Local seeing	Primary mirror (0.09″) Caisson (0.11″) Tube (0.15″) Cage (0.08″) Slit (0.10″) Wind (0.08″) Other (dome wake?) (0.25″)	0.43″
Optics	Primary mirror (0.24″) MegaCam (0.08″) Other optics, etc. (0.18″)	0.33″
TOTAL		0.89″

For the feasibility study of IMAKA we set out to (1) confirm the findings from Salmon et al (2009) and Chun et al. (2009) using an optical turbulence profiler on the CFHT telescope and (2) to quantify the spatial and temporal characteristics of the optical turbulence in and just outside the dome for input into the `IMAKA performance simulations/error budget. To do this we've begun a two-staged experiment. The first phase of the optical turbulence profiler (OTP), now deployed at a bent-Cassegrain port on CFHT, consists of a single Shack-Hartmann wavefront sensor that measures the wavefront tilts over a one-meter off-axis portion of the CFHT primary. The different turbulence layers have very different velocities so with this system we separate the various layer contributions temporally. The results from this experiment are given in this section. In the second

phase of OTP, we will deploy a true profiler which uses multiple stars to directly triangulate the altitude of the turbulence layers. This is planned for later this year.

In addition, we note that there are now additional profilers and seeing monitors on the summit. There are two seeing monitors on the summit of Mauna Kea: the CFHT DIMM in the slit of the CFHT enclosure and the summit facility Mauna Kea Atmospheric Monitor (MKAM). MKAM is a low-resolution optical turbulence profiler and seeing monitor (MASS/DIMM) sited at the location of the old CFHT/Gemini weather tower. This facility now provides the strength and distribution of atmospheric seeing on a nightly basis. Over the course of the first few months of data with MKAM the median MASS seeing (essentially free-atmosphere seeing as it is measured from 500m and above) was measured to be 0.3". This is in excellent agreement with past studies at Mauna Kea. In addition, a high-resolution optical profiler (Lunar SHABAR) is being deployed in a campaign mode on the summit by Paul Hickson/Thomas Pfrommer (UBC) and will provide very high resolution profiles from inside the dome and at the MKAM site.

This section of the report provides the results from the first phase of OTP (single-star WFS). While observations are still being collected, we already see that the technique provides the means to separate the layers and quantify their relative contribution.

4.2 OTP Summary

1. An optical turbulence profilers (OTP) has been deployed at the bent-Cassegrain port of CFHT and observes, typically for 15 minutes, on nights when ESPANDONS queue observations are made. With the single star WFS we can estimate the total phase variance and the relative strengths of the turbulence inside and outside the enclosure.

2. The optical turbulence measured by OTP within the dome is significant and often the dominant contribution. On average we find over the 56 nights sampled to date that the low-temporal frequency component ($f<1$Hz) is equal to or even slightly larger than the high-frequency component ($f>1$Hz). All studies (here with OTP, Salmon et al (2009), and Racine et al. (1991) give similar fractions of contributions from the dome and atmosphere.

3. We plan to continue taking data through 2010A with a detailed analysis during the summer 2010. We hope to extend the study into 2010B to sample a full year of conditions and take full advantage of data from the CFHT (slit) DIMM, the newly commissioned Mauna Kea Atmospheric Monitor (MKAM), and the yet to be deployed Lunar-SHABAR.

4. A key step needed is to deploy a full SLODAR/LOLAS instrument for CFHT later this year. These true profilers will obtain the turbulence altitudes directly and will help to remove any final ambiguities in the altitude of the turbulence.

4.3 OTP

The OTP campaign is a collaboration between CFHT, the Institute for Astronomy at the University of Hawaii (M. Chun), Durham University (R. Wilson and T. Butterley), and Universidad Nacional Auton'oma de Mexico (UNAM) (R. Avila). The experiment consists of a 20x20 Shack-Hartmann wavefront sensor (WFS) imaging a 1-meter off-axis portion of the primary mirror (Figures 21a,b). The observations consist of a series of WFS images from a bright single star taken at the Cassegrain

focus of the telescope over approximately a 15 minute period. Observations are made on nights when queue observing is made with the ESPADONS spectrograph and the star is acquired in the general direction of the last ESPADONS observation. Generally only one data set is obtained per night.

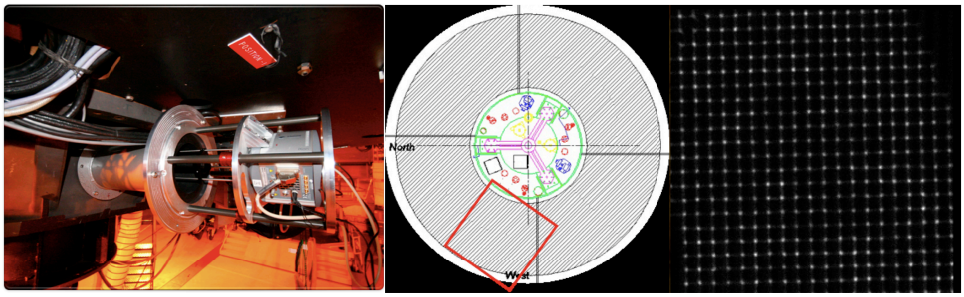

Figure 21: Version 1 of OTP on CFHT. OTP is a 20x20 Shack-Hartmann wavefront sensor mounted to the bent-Cassegrain port (left) images an approximately 1-meter portion of the primary mirror (middle). Sequences of spot images (right) are saved and reduced to centroids and intensities.

OTP was installed on the telescope in July 2009 has been operated by CFHT staff (OAs) during ESPADONs runs and data sets, approximately 15 minutes long, have been collected on 56 nights over the last nine months. The images (Figure 21c) consist of a roughly square array of 20 x 20 star images (one from each of the 5-centimeter subapertures of the wavefront sensor). Data sequences at a frame rate of about 55Hz are taken over a period of about 15 minutes. Each image is reduced to a set of wavefront gradients (spot centroids) and intensities (spot fluxes). These in turn are used to calculate the wavefront phase (global tilt removed), slope cross-covariance arrays, and subaperture scintillation (spot intensities). The pipeline data reduction is done automatically the following day.

4.4 Data Analysis

`IMAKA depends critically on the distribution of optical turbulence along the line of sight. To this end, we felt it was imperative that we reconfirm the results of Salmon et al (2009), Racine (1991), and Chun et al. (2009). With OTPv1, however, we must make the fundamental assumption that the dome seeing and atmospheric seeing have distinct characteristic temporal frequencies. We find that that this is very likely the case.

4.4.1 Cross-covariances

The cross-covariance (or cross-correlation) maps of the slopes or phases show phase aberrations with distinct velocities. An example of the slope cross covariance function in Figure 22. These are the average cross covariance of the x-slopes within a single data packet (roughly 1000 samples). The zero time-step cross covariance is the autocovariance. In the cross-covariance maps, layers moving at different velocities show up as covariance 'peaks' that are displaced from the origin. The integral under any one of the covariance peaks is the total variance in slope-space from each of the layers while the shape of the covariance peaks is related to the shape of the phase spatial power spectrum. The cross-covariances, or cross-correlation of f(x,y,t) and f(x,y,t+dt), provides a simple means to distinguish the dominant contributing layers. Layers moving quickly across the line of sight, result in a cross-correlation peak that is quickly displaced from the center of the correlation map while stationary layers or layers with little or no motion across the line of sight contribute to

the central correlation peak.

In general most of the phase cross-correlation maps show a very strong near-zero velocity component and one or two layers moving across the line of sight. An example of a particularly clear case is shown in Figure 22. In these data, the atmospheric layers (one moving quickly and one moving slowly) are easily seen in a sequence of slope cross-correlations with increasing time delays.

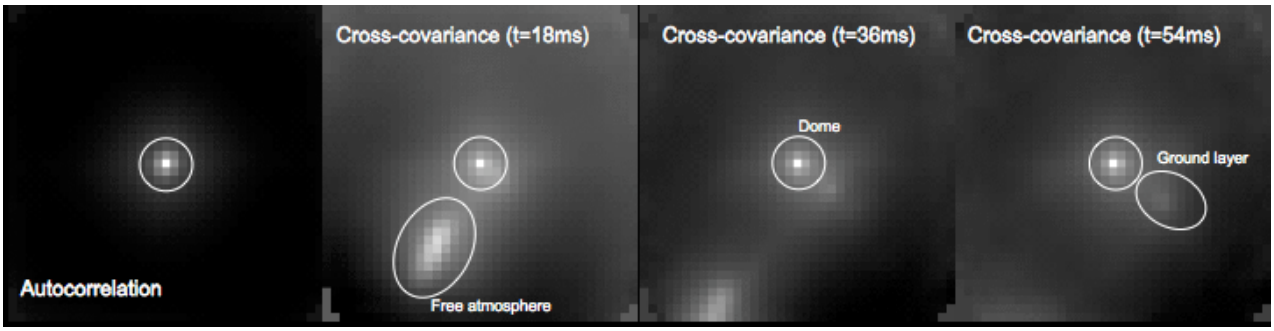

Figure 22: OTP slope covariance maps: A sequence of wavefront slope cross covariances from 6 July 2009. Each image is the average of the x-slope and y-slope cross covariances within a single 15-minute data set for time delays of dt=0 (autocovariance), 18, 36, and 54 msec (cross-covariances) steps. The sequence clearly shows three dominant layers with three distinct velocities. The high-speed layer, moving at roughly 30 m/s towards the bottom left, is a high-altitude layer while, the slower-speed layer (~7 m/s) is likely the ground-layer just outside the dome. These two layers are also seen in a full-atmosphere turbulence profiler that was running concurrently on the Coude roof of the UH2.2m telescope. The final layer has a nearly zero velocity and is likely the turbulence within the enclosure. Each image in the sequence is auto-scaled to the intensity of the peak in the cross covariance.

Since the observations are made using a single-star, there is no triangulation, as with SCIDAR or SLODAR, to definitively identify the layer's altitude. Rather, we must depend on the velocities of the correlation peaks to distinguish the layers. From the sequence of slope cross-covariances shown in Figure 22 we have confidence that the near-zero velocity layer arises within the dome since data from a full-atmosphere optical turbulence profiler (iSLODAR) running on the UH2.2m Coude roof during the first OTP run showed similar atmospheric layers but little or no near-zero velocity layer (following figure).

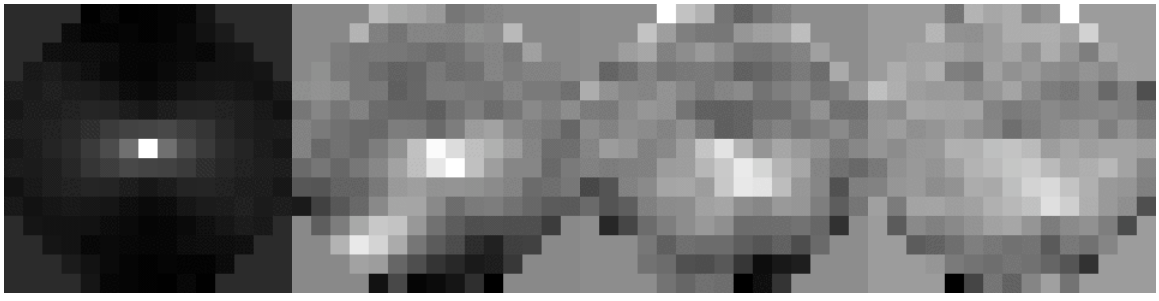

Figure 23: Full-atmosphere SLODAR (iSLODAR) slope covariance maps for times that match the covariance images shown in Figure 22. Note that the two atmospheric layers in the iSLODAR covariance maps match those in the OTP covariance maps but importantly iSLODAR does not show the zero-velocity layer. As in Figure 22 the maps show the autocovariance, then the cross-covariances for time steps of 1, 2, then 3 time steps. The layer velocities derived from iSLODAR and OTP are comparable.

While Figure 22 clearly shows our ability to separate turbulent layers with OTP, the majority of data shows a wavefront phase variance dominated by the zero-velocity "enclosure seeing". In nearly all of the data taken during the first run, this "enclosure seeing" is a significant contribution. The correlation time of this turbulence is extremely long (orders of magnitude longer than the atmospheric (external) phase correlation time).

4.4.2 Wavefront Phase Variance and relative contributions

An important measure to quantify is the total wavefront phase variance that arises from within the dome and from outside the dome. These, along with the spatial spectrum of phase aberrations determine how the phase aberrations degrade the delivered image quality at the telescope focal plane. Since the layers show such distinct temporal signatures, one way of determining the contributions of each of the components is via the temporal phase power spectrum.

We adopt a model of discrete layers giving rise to the optical turbulence and then fit a set of template power spectra to the measured temporal phase power spectra. In this analysis we used the power spectrum of a wavefront decomposition into Zernikes. Zernike coefficients for the first few radial orders were reconstructed from the slope vector maps. The average power spectra of the astigmatism terms (Z5 and Z6) for each night (roughly 15-25 minutes of data) were then fit using the theoretical single-layer Zernike power spectra (Roddier et al 1995). Five layers were fit to the power spectra using a CLEAN-type algorithm where successively weaker peaks in the f*PSD vs. log(f) function are fit and removed with the theoretical templates. The fit was allowed to shift the template in log-frequency and in amplitude (power). Examples are shown in Figure 25 below.

With the results of the layer fits, we then cut the layers into two regions: those with a characteristic frequencies less than 1Hz and those with frequencies greater than 1Hz. The choice of the cutoff frequency was made arbitrarily but was roughly mid way between the two most common prominent peaks. The low frequency component has a characteristic frequency of about 1/10 Hz which corresponds to a transverse wind speed that is considerably lower than the median wind speed on the summit (~6-7 m/s) so we attribute the low-frequency components to local/dome seeing.

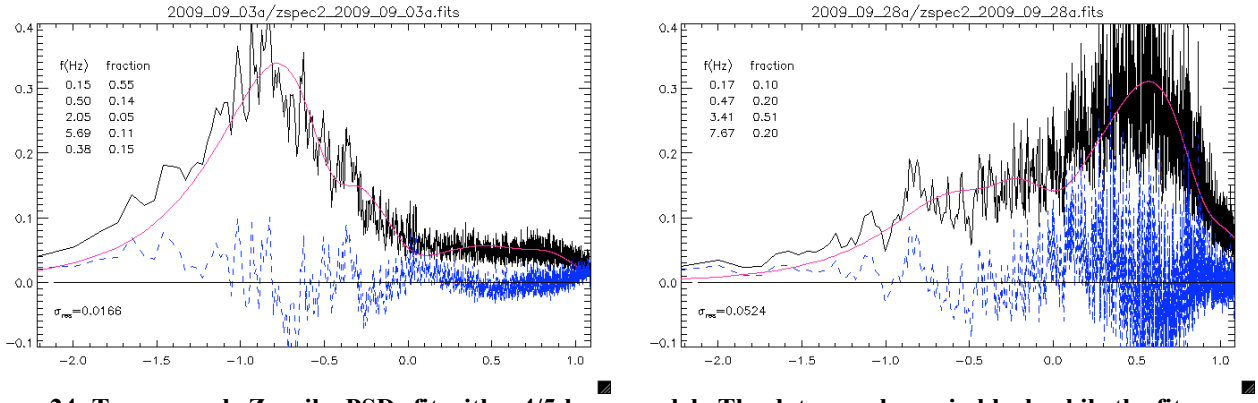

Figure 24: Two example Zernike PSDs fit with a 4/5-layer model. The data are shown in black while the fits are shown in red. The data is shown in f*psd(f) versus log(f) as in Roddier et al. (1995). The area under the curves are proportional to the total variance in the layer. The blue curve shows the residual after the model fit. The two nights show dramatically different distributions in frequency space. The 2009-09-03 data appears to be nearly entirely due to dome seeing while the atmospheric seeing dominates in the 2009-09-28 data set.

For each data set we also calculated an integrated wavefront variance and an r_0 value. Armed with this and the relative contribution of the 'dome' and 'atmospheric' seeing, we generated a distribution of integrated seeing and the relative contributions from the dome and the atmosphere. These are shown in the figure below.

It is clear from the data taken to date with OTPv1 that the dome seeing is comparable if not worse than the atmospheric seeing. The median atmospheric seeing (0.43") and the median dome seeing (0.51") are very comparable to that found by Salmon et al (2009) though with the dome seeing being worse in this data set. We note that our choice of cutoff frequency influences the balance of the two components (they are equal at $f_{cutoff} = 0.8$Hz) so at this point we simply conclude that the "dome" and "atmosphere" components are essentially equal in strength. Interestingly from the data taken so far it appears the when the total integrated seeing is poor, it is predominantly due to poor dome seeing.

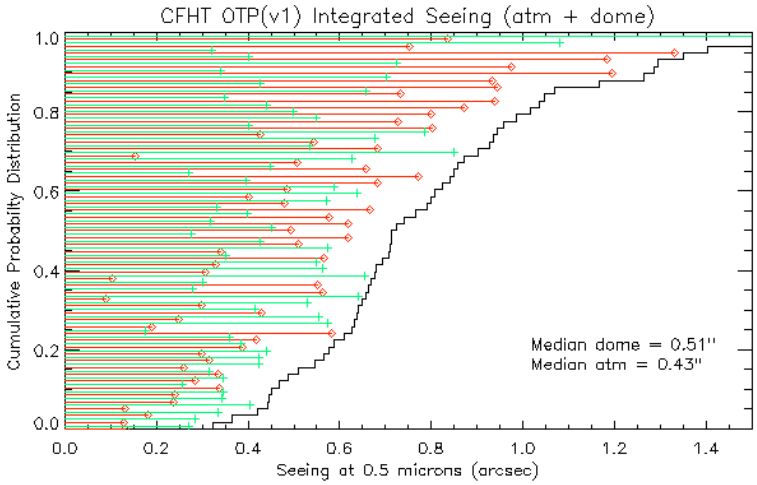

Figure 25: Cumulative distribution of integrated seeing for the OTPv1 data set. For each data set, a value of the total seeing (curve), dome seeing (red), and atmosphere seeing (green) are displayed.

Data will continue to be taken with OTP and this summer we will upgrade to OTPv2 which will be a combination SLODAR/LOLAS. Triangulation using multiple stars will remove the ambiguities in layer altitudes we have now. Nonetheless the results from OTPv1 are consistent with the Salmon et al (2009) results for MegaCam data and suggest that a GLAO system will (1) remove a large portion of the total optical turbulence and (2) will not need to run at a very high temporal sampling rate.

4.5 Dome venting

The OTPv1 results agree with Salmon et al (2009) and Racine (1991) and indicate that seeing generated in and around the dome environment often plays a decisive role in degrading CFHT image quality. Whether these effects come from seeing local near the primary mirror, generalized turbulence in the dome or from the mixing of air masses near the dome skin's external boundary layer, the fact that they originate very close to the telescope suggests that their removal will considerably enhance IMAKA's GLAO performance.

Almost all major 4-m class telescopes have retroactively installed dome vents with decidedly beneficial effect on image quality. It is, however, frustratingly difficult to obtain quantitative data on this from other facilities. Detailed studies at CFHT by Racine et al (2010) suggest that the addition of vents should remove a considerable portion of a 0.4 arcsecond contribution to the current median value of 0.89 arcsec. As a result of these studies, the CFHT Board has authorized the development and installation of dome vents with the intent of having them in operation by 2013.

We note that dome venting alone will not deliver the image qualities expected from `IMAKA. Residual dome seeing, mirror figure, optical aberrations within MegaCam, and other local sources of image degradation will remain. Dome venting is however an important component to achieving the full `IMAKA performance.

5. Performance Simulations

5.1 Introduction

In this section we present the results of the `IMAKA performance simulations. The feasibility study developed a new simulation code that incorporates a numbers of unique features specifically for `IMAKA. These include a model of the atmospheric turbulence based on the Gemini Mauna Kea Ground-layer study, the effects of misconjugating and tilting a DM with respect to the optical axis, and the effects of the tip/tilt correction from an orthogonal-transfer CCD camera. The code (instant_GLAO) was developed by Olivier Lai and has been extensively cross-compared with the yao and simul codes (Francois Rigaut), the LAOS code (Brent Ellerbroek/Luc Gilles), and PAOLA (Laurent Jollisaint) for a number of case studies. In addition, PAOLA has been modified to be used with `IMAKA and is now being used to develop a detailed baseline for the GLAO system .

5.2 Summary of `IMAKA simulations:

Key performance simulation results are as follows:

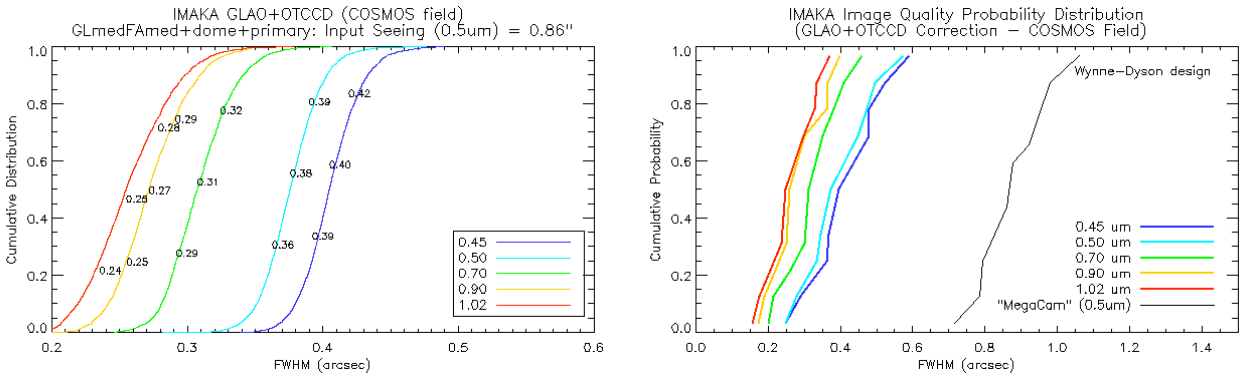

Figure 26: Summary plots of the `IMAKA performance estimates. Figure on the left shows the variation of the FWHM across a one-degree diameter field of view. Figure on the right shows the probability distribution of obtaining a particular FWHM over the range of seeing considered.

1. Developed a Monte-Carlo simulation code (instant_GLAO) specifically for `IMAKA studies that includes more sophisticated algorithms and detailed errors. With instant_GLAO we have quantified the phase errors due to the tilt of the DM with respect to the optical axis and the optical conjugation of the DM with respect to the optical turbulence. ***These errors place strong constraints on the `IMAKA optical design and drove the optical design away from an adaptive secondary.***

2. An estimate of the dome seeing, the primary mirror figure, and the optical aberrations of the `IMAKA optical design are included in the simulations. The CFHT dome seeing (Salmon et al. 2009) results in a significant degradation to the delivered performance of `IMAKA and the effort to reduce the locally generated seeing is a key element to the `IMAKA development. Note however that ***while dome venting is being actively pursued, we have pessimistically maintained the full dome seeing in the `IMAKA performance simulations***.

Table: `IMAKA End-to-End performance for the Wynne Dyson design in median/median atmospheric conditions including dome seeing and the primary mirror figure. The table shows the 20%, 50%, and 80%-tile FWHM over the one deg diameter FOV for five wavelengths of interest with full GLAO+OTCCD correction. For reference, the input integrated seeing was 0.86" at 500 nm.

Wavelength (filter)	GLAO+Full OTCCD
0.45 microns (b)	0.39, 0.40, 0.42"
0.5 microns (g)	0.36, 0.38, 0.39"
0.7 microns (r,i)	0.29, 0.31, 0.32"
0.9 microns (i,z)	0.25, 0.27, 0.29"
1.0 microns (Y)	0.24, 0.25, 0.28"

3. We now run performance estimates for a range of optical turbulence profiles and we use these to construct an estimate of the probability distribution of the delivered performance (see for example Figure 26). The median performance estimates for the delivered FWHM of `IMAKA are still 0.3" but only at the redder wavelengths (0.7 microns and longer).

4. The large field of `IMAKA works to its advantage as it is found that there is a >95% probability of finding a sufficient number of guide stars within one square degree at the North Galactic Pole (NGP) for the GLAO correction. The sky coverage will be largely driven by the requirement of tip/tilt guide stars for the OTCCD correction and is estimated to be around 60-70% at the NGP.

5.3 Inputs to the simulations

GLAO over these very large fields of view is very sensitive to the input turbulence profile near the ground. The ratio of ground layer turbulence to free atmosphere turbulence determines the overall maximum gain achievable by GLAO, while the distribution of the local turbulence determines the corrected field of view. As a canonical case, we adopted the "standard" Mauna Kea Turbulence profile near the ground, as measured and reported by M. Chun for the Gemini GLAO study and a limited set of Generalized-SCIDAR data taken at the UH2.2m for the upper atmosphere layers. We note that as a simplification in instant_GLAO, we have moved the upper-most free-atmosphere layer to 3000-meters. The layers are given in terms of their relative strength at a given altitude; a model of the atmosphere is then created by generating as many phase screens as there are layers and normalizing them to a chosen r_0 per layer such that the sum of the phase screens gives the required D/r_0.

Table 9: Standard Mauna Kea Turbulence profile. Note that the layer speed is not used in the `instant_GLAO.pro` code: One of the major simplifying assumptions of this program is that the temporal error, can be made much smaller than the other error terms.

Altitude (m)	Fractional Strength	Speed
0	0.295	6.5 m/s
15	0.141	6.5 m/s
30	0.039	6.5 m/s
80	0.020	6.5 m/s
280	0.024	6.5 m/s
1000	0.290	15.0 m/s
12000 (*~3000m*)	0.191	30.0 m/s

To understand the performance under conditions other than the median GL and median FA, we also ran the simulations for the 25% and 75% GL and FA integrated strengths. The ground layer and free atmosphere strengths were found to be uncorrelated (Chun et al. 2009) so these strengths provide nine (e.g. 3x3) representative cases for the simulations. The median ground layer/median free atmosphere cases is equivalent to the standard MK profile. The dome seeing is obtained from Salmon et al, 2009, which is quoted as 0.43" at 500nm. The dome seeing's main characteristic (see OTP section) is its very long correlation times. Since instant_GLAO does not take temporal aspects into account, the way dome seeing is simulated is by adding a Kolmogorov phase screen at zero altitude with r_0=0.24m and L_0=30m. The degradation due to the primary mirror can also be included and we use a phase map estimated by a 64x64 Shack Hartmann obtained in 2004 by Salmon et al. The primary mirror aberrations are implemented in instant_GLAO by adding this constant phase term to the pupil. The inputs seeing values for the nine cases (good/good to bad/bad) are detailed in Table 9, showing the contribution of the ground layer (with and without dome seeing), the free atmosphere, the total seeing (with and without dome seeing).

From Table 9 above, we see that the median/median case with dome seeing give 0.86" at 500 nm; if we add the contribution of the optics, this gives us a number very close to the measured median Megacam IQ of 0.91". It should be noted that the values used here do not entirely agree with Salmon et al. (2009). For example the median atmospheric seeing corresponds to 0.68" while Salmon et al give a value of 0.55". We note however, when including the dome seeing, the total seeing is very close to the 'median' value given in Salmon et al. (2009). In this respect, when the assumption is made that `IMAKA must deal with the current extent of dome seeing, the simulation inputs are realistic but our atmosphere-only cases may be pessimistic.

Table 10: Seeing conditions for the nine adopted profiles: Good, median and bad values of seeing (at 500nm) for the nine combinations of 25%, 50%, and 75% ground layer (GL) and free atmosphere (FA) .

		Good FA (0.31")	Median FA (0.42")	Bad FA (0.55")
Good GL (0.35")	Total atmospheric seeing	0.503"	0.589"	0.698"
	with dome seeing	***0.715"***	***0.785"***	***0.877"***
Median GL (0.47")	Total atmospheric seeing	0.600"	0.677"	0.778"
	with dome seeing	***0.794"***	***0.860"***	***0.947"***
Bad GL (0.64")	Total atmospheric seeing	0.749"	0.817"	0.906"
	with dome seeing	***0.921"***	***0.981"***	***1.060"***

To get an idea of the frequency of the performance gains of 'IMAKA, we assigned rough probabilities to each of the 9 cases in the same way as what was done for the Gemini GLAO feasibility study (Andersen et al 2006). These probabilities include two important assumptions. First, that there is little or no covariance in the likelihood of having any given ground and free atmosphere profile (Chun et al 2009). Second, it assumes that the dome seeing is constant under all conditions. This is clearly not the case (Salmon et al. 2009), and surely biases the results somewhat, but until more data on the distribution of dome seeing is available, it is a reasonable assumption to

start with.

Table 11: Rough probabilities for the occurrence of input atmospheric conditions: ***We assigned rough probabilities of encountering any of the nine profiles by assuming that the Good and Bad ground (and free atmosphere) conditions exist about 25% of the time and that the Typical ground (and free atmosphere) conditions exist about 50% of the time. We assume the ground and free atmosphere conditions are entirely uncorrelated.***

Ground Layer	Free Atmosphere		
	Good	Median	Bad
Good	6.25%	12.50%	6.25%
Median	12.50%	25.00%	12.50%
Bad	6.25%	12.50%	6.25%

Lastly, field dependent (chromatic) aberrations due to the optical design can become an important source of error for such large field of view in real systems, especially since the constraints of DM conjugation impose complex solutions to achieve the stringent image quality requirements. These aberrations have been implemented in instant_GLAO, using wavefront phase aberration maps at various field locations exported from the optical design raytrace and interpolated at each location of the required PSFs. These are added whenever end-to-end performance PSFs are computed. Their contribution is very small.

5.4 Simulation tools

`IMAKA poses several challenges to simulating its performance. Principally, `IMAKA's large field size is about 60 times larger than typical AO fields of view. This leads to enormous memory requirements and the necessitates the inclusion of errors terms typical neglected in a classical narrow field of view AO. `IMAKA's delivered image quality is also not a diffraction-limited image and averaging of spectral residuals is considerably slower than for a classical AOS. This plus the fact that many Monte Carle AO simulations include full physical optics WFSing models (e.g. detailed but slow) would require too much computing time to make useful progress. Finally, the `IMAKA concept is a combination of both GLAO and OTCCD corrections and with the exception of instant_GLAO and now PAOLA no other AO simulation tool is set up to handle a combined GLAO and OTCCD correction. These reasons led us to develop a new code. While a considerable effort to develop, instant_GLAO was explicitly written to tackle the detailed problems within `IMAKA. Since the Monte-Carlo approach does not lend itself to all type of studies, we also updated the analytic modeling tool PAOLA to be used with `IMAKA. This allows us to explore quickly general effects (e.g. order of system, variations of the CN2 profile, etc.) quickly with PAOLA but also allows us to develop a deeper understanding of how `IMAKA works with instant_GLAO. Over the course of the study we extensively compared all the tools at our disposal and it is comforting that each of these different tools, which each make different assumptions, all yield approximately the same performance.

5.4.1 Instant_GLAO

The new simulation code `instant_GLAO.pro` was developed specifically for this study. It computes PSFs on a specified grid in a field after correction by a ground-layer adaptive optics system and an Orthogonal-Transfer CCD. Instant_GLAO is a Monte Carlo simulation code based on the geometrical propagation of light through the turbulent atmosphere. The vertical distribution of the turbulence is assumed to be well represented by a discrete set of properly scaled and shifted

phase screens. The phase for each field position is computed by summing the appropriate section of each phase screen. This process is first applied to the direction of the guide stars, and the resulting wavefront measurements are used, either by simple averaging or least square minimization of the residual error, to compute the shape of the deformable mirror. The residual phase (and associated PSF) is then computed by subtracting the DM correcting wavefront from the phase at each PSF field location. A subsequent correction by the OTCCD is to measure the tip-tilt at specified field locations and apply this correction around a specified radius to simulate the elastic focal plane of the OTCCD.

The main simplifying assumption of instant_GLAO is that the temporal error (loop lag, closed loop attenuation, etc) can be made small compared to the residual phase error imposed by the free atmosphere. Therefore, to ensure faster convergence, instant_GLAO neglects temporal effects and draws each new iteration from a completely uncorrelated random phase shift on each phase screen. This is necessary because unlike classical AO simulations where each iteration contributes to an improvement of the estimation of the coherent core, in our GLAO simulation each iteration produces wide speckle patterns that take much longer to average out. A consequence of this is that the measurements are made in open loop, as the phase is measured on the guide stars without any prior knowledge of the deformable mirror.

The end-to-end simulations in instant_GLAO include numerous effects that are described in the appendix. We note here that the combined GLAO+OTCCD correction is made for each iteration and normally, for end-to-end run, we consider the atmosphere, dome, mirror figure, and optical design in the aberrated wavefront as well as the conjugation and/or tilt of the deformable mirror. What is notably missing from the current simulations are a more realistic value for the dome seeing including variations with time and the effect of venting the CFHT enclosure, and possibly implementing a WFS model, the temporal bandwidth, and noise. These however should also lend very well to analysis with PAOLA.

5.4.2 PAOLA

PAOLA (Performance of Adaptive Optics for Large or Little Aperture) is a general purpose AO modeling tool to compute the long exposure AO OTF or PSF in a single shot, including a large number of options and AO modes. It has been continuously developed since 2001 by Laurent Jolissaint (aquilAOptics). This tool has been used for several instrument studies over the past years, and was tested successfully several times against Monte-Carlo codes in all its operational modes, in particular for GLAO. PAOLA makes use of the theoretical relationship between the residual phase spatial frequency power spectrum (PSD) and the long exposure AO OTF, the later being used as an OTF filter applied on the telescope OTF to get the overall telescope+AO OTF. This technique was pioneered by Rigaut et al. (SPIE 3353, 1998) and extended by Jolissaint et al. (JOSA A, 23, 2006). As it is an analytic code, it is fast and a long exposure PSF can be obtained in a couple of second/minutes with a desktop computer.

In the context of IMAKA, this code is used to explore the AO parameter space and determine:

- the number of WFS lenslets, in other words the order of the system
- the number of guide stars
- the limiting magnitude and the optimal WFS integration time (FWHM-based)
- the impact of the OTP variations on the PSF
- the PSF structure with GLAO & OTCCD correction

5.5 `IMAKA basic configuration

5.5.1 Order of the GLAO system

The optimal number of actuators on the deformable mirror or the number of sub-apertures on the wavefront sensor is a trade between delivered image quality, field size/turbulence profile, and sky coverage. The wavefront correction is driven by the shortest wavelengths where the residual wavefront variance has the largest impact on the PSF FWHM but also where the anisoplanatism of the correction is also largest. The performance at short wavelengths (B, V and even R) is improved with a 20x20 with respect to a 10x10 Shack-Hartmann wavefront sensor and we nominally use 20x20 as our baseline system. Increasing the number of subapertures much beyond 25 only slowly improves the performance even at the shortest wavelengths, at the cost of smaller and smaller subapertures which in turn will affect sky coverage (see below).

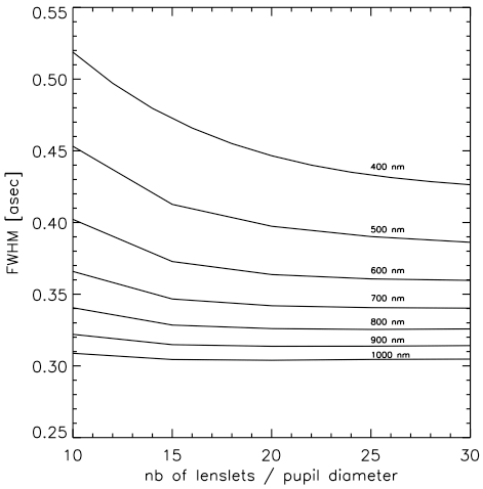

Figure 27: GLAO+OTCCD performance (PAOLA) versus order of GLAO system and wavelength

5.5.2 Number of Guide Stars/Wavefront sensors

The required number of guide stars to obtain a uniform and high-order GLAO correction was explored. We find that the delivered performance in FWHM depends only weakly on the number of guide stars with more guide stars providing a slightly smaller FWHM. This matches the expectation that the wavefront reconstruction will, for bright stars, be dominated by the thinness of the optical turbulence profile. PSF variations across the field, as measured by the standard deviation of the FWHM and the elongation of the PSFs throughout the field, also depends only weakly on the number of guide stars used. This is true even in the case of a non-uniformly distributed set of natural guide stars. To test this, many random guide star asterisms were generated and used with PAOLA: Point spread functions were calculated on a 3x3 grid of locations 20 arcminutes apart. The median FWHM GLAO-only value for an r-band PSF is 0.37” for the 4 random guide stars asterisms, 0.35” for 6 GS and 0.34” for 8 and 10 GS while the variation of the R-band FWHM, as expressed by the standard deviation in FWHM for all the random asterism, is 23mas for the 4 GS asterism, 22mas for 6 GS, 19mas for 8 and 17mas for 10GS. Note that these values exclude PSF locations if they happen to lie within 2' of a GS. This is the area over which the largest PSF variations are found but their exclusion in the 6-GS case amounts to only a few percent of the one degree field of view. They are not representative of the field as a whole. For reference, the default case of a regular hexagonal guide star asterism gives the same FWHM as the 6 random guide stars asterism (0.35”), but the standard deviation of FWHM across this field is only 9mas. The values are given for R-band but simulations at V-band show identical trends but with median FWHMs ~ 0.04” larger.

From this we conclude that for bright guide stars more guide stars provide better correction but that the uniformity of the correction is largely independent of the number of guide stars. The variation of the PSF from the randomly drawn guide star asterisms is worse than the fixed, uniformly-spaced 6-GS case but on average is still very uniform.

5.5.3 Wavefront correction/Deformable Mirror

We found that there are strong constraints on the type of wavefront corrector that can be used in an extreme-GLAO system. In particular, due to the large corrected field size and the thinness of the turbulent layers we are trying to correct, the deformable mirror tilt and conjugation are highly constrained. Using instant_GLAO, we studied the effect of tilting the deformable mirror with respect to the optical axis of the system and the effect of optically conjugating the deformable mirror away from the turbulence. Both effects are described in detail in the appendix. The impact on `IMAKA is as follows:

- the error due to the tilt of the DM drives the system towards a physically larger optical system (larger deformable mirror) with small angles of incidence on the DM,
- the constraint on the conjugation of the DM excludes an adaptive secondary mirror (at least one that would at least roughly resemble the current CFHT secondary).

Quantifying these errors drove the optical design requirements and the selection of the two approaches.

5.5.4 OTCCD correction.

The OTCCD array can be used to correct tip-tilt locally by effectively acting as an elastic focal plane camera. Each 512x512-pixel cell of each chip (covering 50"x50") can serve as either detector real estate for science imaging or can be read at high sub-frame rates (e.g. 100Hz). Areas of the science field containing bright stars can therefore be used to provide a measure of the local tip-tilt. These multiple regions across the full field can be used to retrieve the global tip-tilt or a global map of the instantaneous field distortion due to anisokinteic tip-tilt. This signal is then used to shuffle the charge on the 'science field' from pixel to adjacent pixel (through the orthogonal transfer process) throughout an exposure. This tip/tilt correction corrects for any residual tip-tilt error that may subsist from GLAO and the local tip-tilt due to the free atmosphere ensuring that the incoming photons are integrated within a tight PSF.

This process happens after GLAO correction so the centroid estimation benefits from the tighter core of the `IMAKA PSF, but it happens in open loop, as the tip-tilt is measured independently from the applied correction. This was a strong driver to develop our own code, as this particular configuration is very specific to `IMAKA. In principle in an actual device, the charges can be transferred partially across pixels (fractional pixels) however this has never been implemented in practice and the charge transfer occurs in integer pixels shifts. Both cases were coded in instant_GLAO, but the difference was found to be small, especially after the PSFs are resampled to the 0.1" pixels.

If there are 200 guide stars in the field, approximately 200' square are lost to guiding, a small fraction of the useful field and provides relatively good homogeneity of the PSFs. However, the PSF variation due to tip-tilt correlations may adversely affect some science goals, and it can be reduced by providing a denser mesh of tip-tilt stars at the expense of scientific field of view. So far, this effect has been difficult to study with instant_GLAO due to the limited height of the top layer of the model atmosphere, which artificially increases the isokinetic angle, but will be addressed in future versions of the code.

5.5.5 Baseline system for simulations

For most of the simulations to date we assumed a single baseline system with a 20x20 actuators DM conjugated to the ground, 6 GLAO WFS/guide stars evenly distributed on a 20 arcminute radius circle, and 180 OTCCD guide stars randomly distributed about the field The detailed design of the subsystems will be explored with the PAOLA simulation tool and is key element of the next phase of the design.

Table 12: ***Summary of baseline 'IMAKA parameters***

Quantity	Value
Telescope	3.6 m telescope with 0.421 m central obscuration
Seeing	0.86" atmosphere seeing (median/median)
Atmosphere	r_0 = 0.152 meters at 500nm (median/median)
Dome	r_0 = 0.234 meters at 500nm
Mirror Figure	as per prime focus measurements (~300nm)
GLAO	
Correction order	20x20 GLAO system (0.18 cm actuator/subap)
Wavefront sensing	6 WFS on 20 arcmin ring with bright guide stars (very little WFS noise)
OTCCD	
Guide stars	~180 distributed randomly about the field (also bright)
Simulation	
Iterations	1000 realizations
output PSFs	60x60 PSFs on 1x1 deg^2 FOV at wavelengths of 450, 500, 700, 900, 1020 nm

5.6 `IMAKA performance

The simulations and performance calculations have steadily improved over the course of the study and now include all of the large sources of error in the input and corrected wavefronts. There are still unknowns in the estimates: "What will be the effect of venting the dome?", "How will the alignment and manufacturing imperfections degrade the performance?". Some of these will work to improve performance, some will work to degrade performance. However, at the level of a feasibility study we believe we know what the fundamental limitations on `IMAKA's performance are. We are encouraged that the estimated performance is largely unchanged from our initial estimates but we note that this too is a reflection of our improved understanding of basic limitations of GLAO and engineering trades (e.g. the move away from an adaptive secondary design). The simulation results should be considered within this context. Further progress will require a larger effort with in-depth system design trades of a Phase A study.

5.6.1 What is the end-to-end performance? How does the performance vary with wavelength?

The end-to-end numbers are shown in the Table below. They are very similar to the 'end-to-end' numbers we quoted in the original study. While we now include dome seeing, mirror figure, and the tilt of the DM we also changed away from the concept based on a misconjugated adaptive secondary. These effects largely balance each other though at the bluest wavelengths the increase in the total seeing included in the simulations degrades the performance significantly. We are also now including Y-band (1.0 microns) in the simulation runs as it was identified as an important bandpass for the science cases.

Table: `IMAKA End-to-End performance for the Wynne Dyson design in median/median atmospheric conditions, including dome seeing and the primary mirror figure. The table shows the 20%, 50%, and 80%-tile FWHM over the one deg diameter FOV for five wavelengths of interest. For reference the input seeing (atmosphere+local) is 0.86" at 500nm.

Wavelength (filter)	GLAO-only	GLAO+Full OTCCD
0.45 microns (b)	0.47, 0.49, 0.50"	0.39, 0.40, 0.42"
0.5 microns (g)	0.44, 0.46, 0.48"	0.36, 0.38, 0.39"
0.7 microns (r,i)	0.38, 0.40, 0.41"	0.29, 0.31, 0.32"
0.9 microns (i,z)	0.35, 0.36, 0.38"	0.25, 0.27, 0.29"
1.0 microns (Y)	0.34, 0.35, 0.37"	0.24, 0.25, 0.28"

In some fields there will not be enough guide stars for full OTCCD correction over the field of view. In these cases the performance will be somewhere between the GLAO-only and full GLAO+OTCCD cases. The GLAO-only FWHM are also shown in the End-to-End performance table. The OTCCD correction amounts to about 0.1" in FWHM at all wavelengths. The additional gains from the OTCCD are clear. A comparison of the GLAO-only and the GLAO+OTCCD PSF FWHM across the field seems to point to the OTCCD contributing in two ways. First it removes the tip and tilt from the upper atmospheric layers. Second, it smooths out the GLAO performance by correcting for tilt anisoplanatism in the GLAO correction. We note that the OTCCD performance across the field depends on the altitude of the free-atmosphere layers and on how we combine information from multiple OTCCD guide stars to generate the correction signal. This will be pursued in more depth in the Phase A study. We will also be using the MKAM MASS/DIMM seeing monitor to develop a better turbulence model of for the free atmosphere.

5.6.2 What will `IMAKA produce for a distribution of guide stars in a real-field?

While most of the simulations made to date used a uniformly distributed asterism of GLAO guide stars, the results presented above and in the rest of this section were calculated for a constellation of GLAO and OTCCD guide stars taken from a *representative* science field. Here we chose the COSMOS field (http://cosmos.astro.caltech.edu/) due to its importance as a field for extra-galactic studies and its modest galactic latitude (~40 degrees). For this field we found ample guide stars for both GLAO and OTCCD correction within the IMAKA field of view.

5.6.3 How does the performance vary across the field?

The performance, as measured by the FWHM, is remarkably uniform over the one degree field of view. For the COSMOS field, eight GLAO guide stars were found near the periphery of the field and over 130 OTCCD guide stars were found within the one-degree diameter field of view. Figure 28 below shows a color-coding of the FWHM derived from an array of 60x60 PSFs (PSFs sampled every one arcminute) across the field. Positions of the eight GLAO guide stars are indicated by yellow stars while the OTCCD guide star positions are indicated by crosses. With an OTCCD focal-plane populated with OTCCDs the detector real estate immediately surrounding an OTCCD guide star is used for sensing the jitter correction. As such, these areas are not accessible for science. The area lost to the OTCCD guide stars is about 1 square arcminute per guide star so in the case of the COSMOS field, this amounts to less than 5% of the field. In addition, the areas surrounding the GLAO guide stars will be vignetted by the GLAO WFS probe arms. These areas

are also not accessible for science. The area vignetted by the WFS patrol arms will depend on the design of the WFS arms but the intent is to minimize this obstruction.

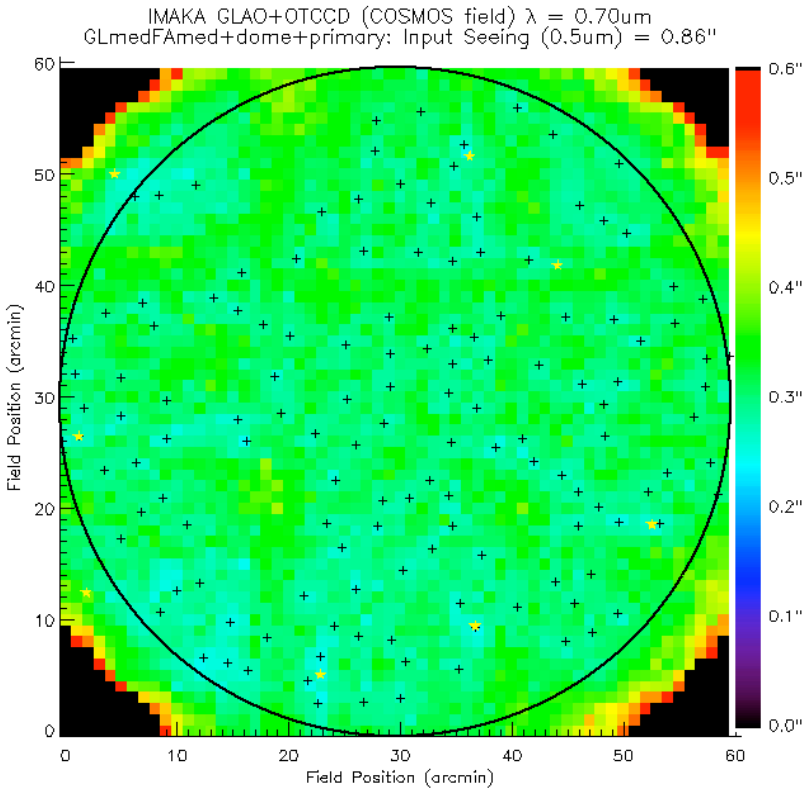

Figure 28: Distribution of FWHM across the one square degree field at an imaging wavelength of 0.7 microns for median/median ground-layer and free-atmosphere strengths. The one degree diameter field of `IMAKA is shown as well as the positions of the GLAO guide stars (yellow stars) and OTCCD guide stars (crosses)

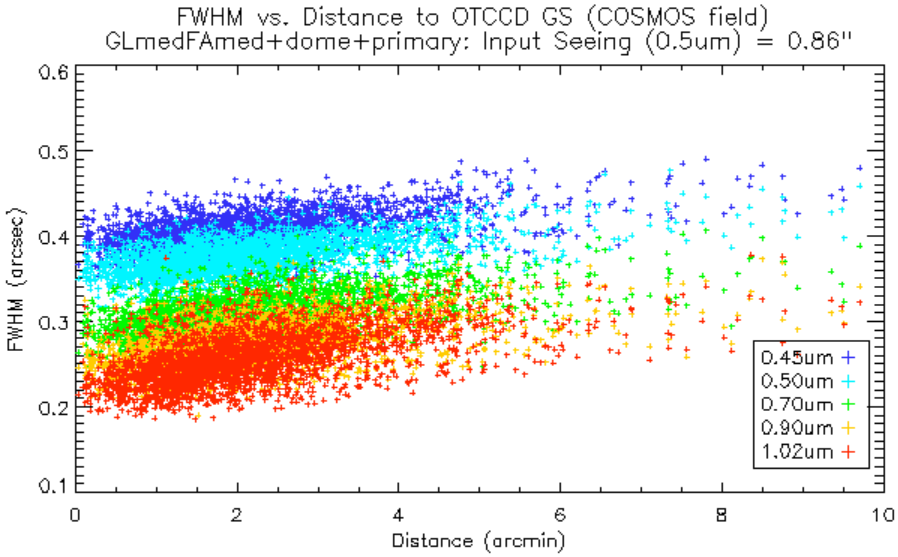

Figure 29: Variation of the FWHM as a function of distance from the OTCCD guide star.

The distribution of FWHM within the one-degree diameter field of view is shown below in the cumulative distribution below for the median/median GL and FA case. Note that the input atmosphere has a seeing of 0.86" at 500nm close to the median delivered image quality of MegaCam.

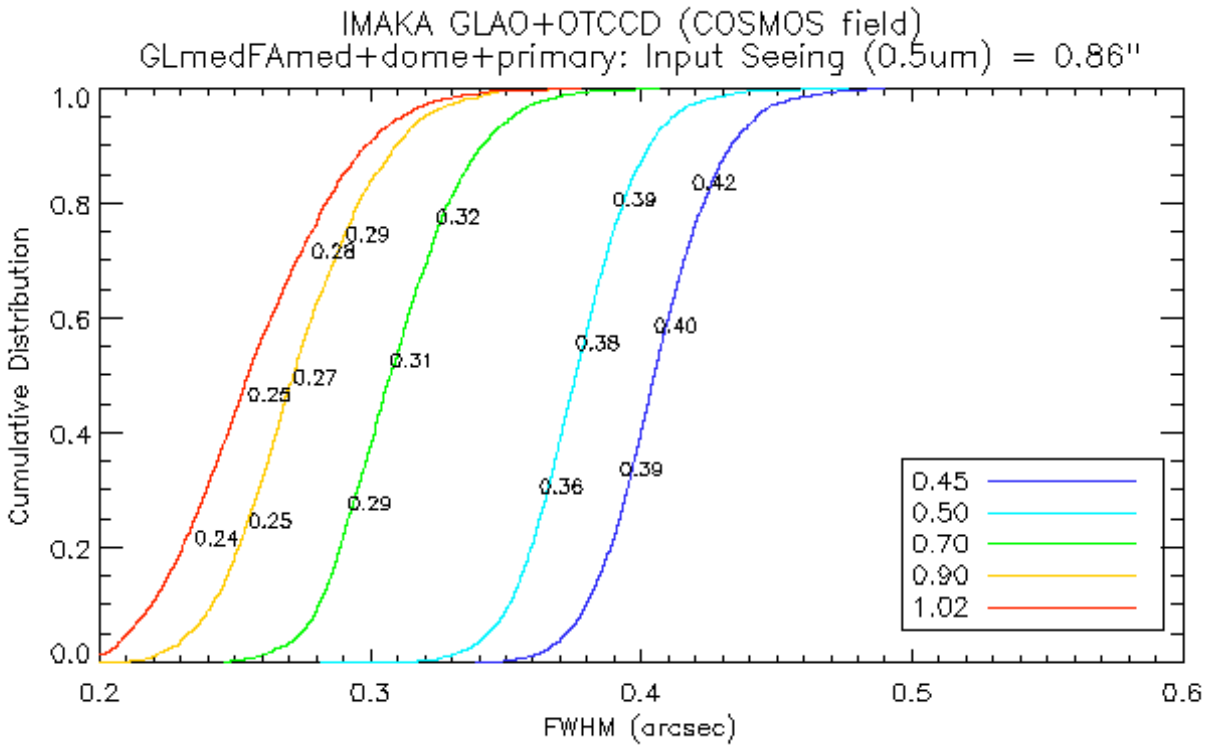

Figure 30: Distribution of FWHM over the one degree diameter field of view for median/median conditions.

5.6.4 What is the probability that `IMAKA will achieve this performance for any particular position in the sky?

Simulation runs using PAOLA suggest that the GLAO correction from a 20x20 subaperture system can be maintained down to a limiting magnitude of V=14 without degradation to the image FWHM. With this, we can determine a 'sky coverage' based on the distribution of stars as a function of galactic latitude.

The sky coverage was determined by estimating the probability of finding at least *n* stars brighter than magnitude *m*:

$$P(m, > n) = 1 - \sum_{i=1}^{n} (\mu(m))^i \frac{e^{-\mu(m)}}{i!}$$

where mu*(m)* is the mean star density of magnitude

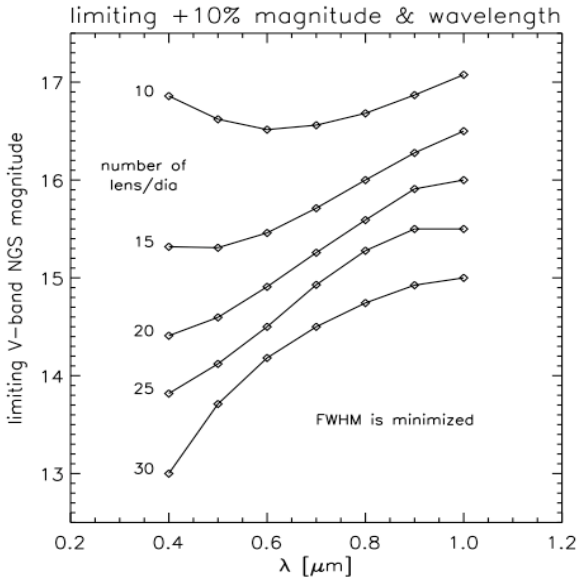

Figure 31: Limiting magnitude versus wavelength and number of subapertures if we allow a 10% increase in the base performance. PAOLA simulation optimizing the bandwidth for the best FWHM.

m from the Besançon model of star counts for a field of view of 1 degree (r=30'). The very large field of `IMAKA works to its advantage as it is found that there is a >95% probability of finding 6-8 stars of m_R<12 within one square degree at the North Galactic Pole (Figure below).

With currently available CCD detectors, a GLAO system with six 20x20 Shack-Hartmann WFSs provides full sky coverage with no degradation to the image FWHM.

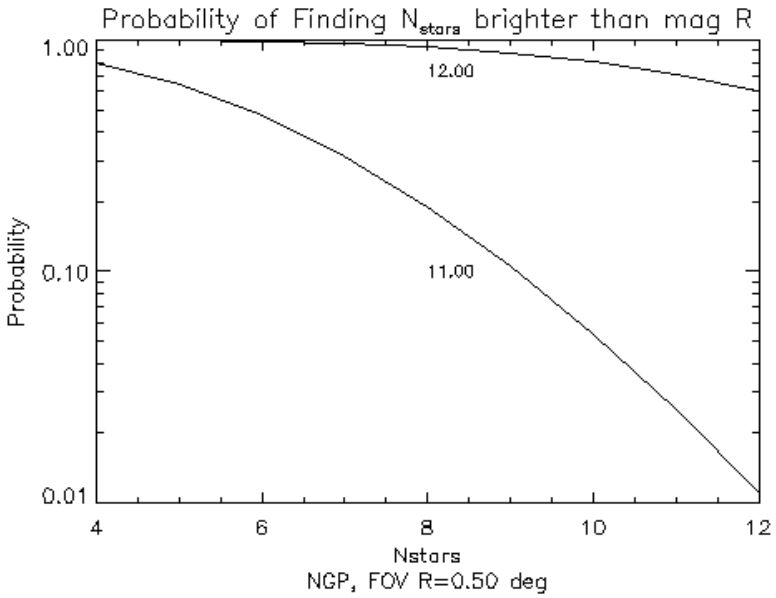

Figure 32: Estimated number of guide stars available for wavefront sensing at North Galactic pole. The probability of finding 8 stars brighter than magntiude R<12 within a degree is high enough to ensure very high sky coverage.

In its actual implementation, there will be additional limitations, such as vignetting of the science beam, location of the WFSs, and mechanical constraints, that will limit the positions within the field where a guide star can be acquired and what the required brightness is. However, it is evident from the calculations above that there is margin in the GLAO sky coverage. This will be explored further in detail during the Phase A.

The sky coverage of the full GLAO+OTCCD correction is limited more by the requirement of a tip/tilt guide star for the focal plane correction by the OTCCD. Assuming that a new OTCCD guide star is needed every 6 arcminutes and a conservative (not optimized) limiting magnitude for the OTCCD GS of 14.5 gives a sky coverage of about 60-70% at the NGP. This corresponds to a sky density of about 100 appropriately bright guide stars within the one-degree field of view.

5.6.5 How does this performance change with seeing? What is the probability that on any particular night IMAKA will achieve that level of performance?

Using the 25%, 50%, and 75%-tile GL and FA strengths and the fact that they are uncorrelated, we generated nine input atmospheric seeing conditions. These range from 0.5" to 0.9" at 0.5 microns. The vertical distribution of the layers, however, was not changed between cases. With these nine cases and their associated probabilities of occurring, we found the following distributions of `IMAKA FWHM (Table and Figure below)

Table 13: Performance as a function input atmospheric conditions*: The cumulative distribution of predicted image FWHM from GLAO+OTCCD correction and their rough probabilities based on the distribution of ground-layer and free-atmosphere seeing from the Gemini MK Ground-Layer study (Chun et al. 2009)*

Probability	0.45um	0.5um	0.7um	0.9um	1.0um
20%	0.37”	0.35”	0.26”	0.22”	0.21”
50%	0.40”	0.37”	0.31”	0.26”	0.25”
80%	0.48”	0.47”	0.38”	0.36”	0.33”

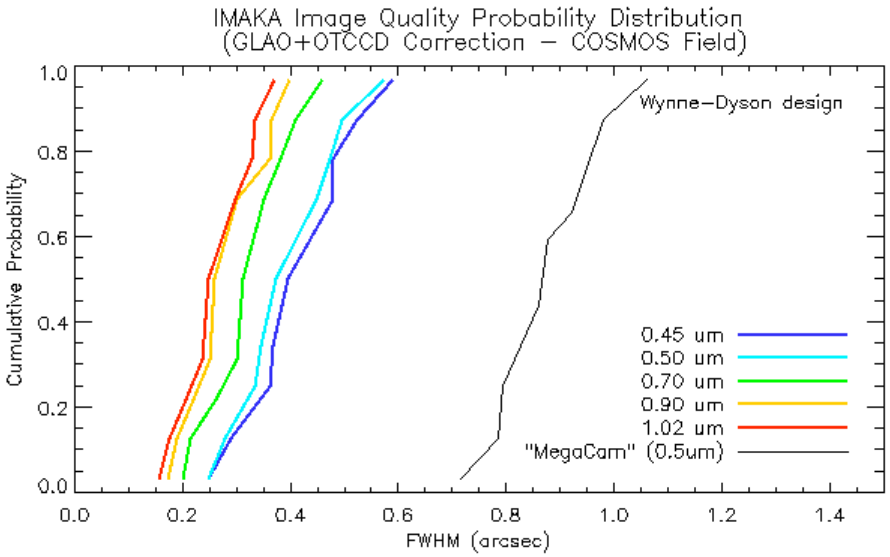

Figure 33: Cumulative probability distribution of `IMAKA image quality for all input seeing conditions used.

Note that the 80%-tile conditions are relatively “poor” at the bluest wavelengths. However, during these times, the resolution at the reddest wavelengths is still excellent and better than the best MegaCam image *ever* taken (e.g. FWHM~ 0.37” in i-band).

5.6.6 How does the performance vary from exposure to exposure?

The atmospheric seeing changes on timescales of order or less than the typical total integration times expected for many of the `IMAKA science cases. As a measure of the sensitivity of the IMAKA delivered image quality to these changes we ran the PAOLA simulation tool on a variety of turbulence profiles. For each profile in the Gemini Mauna Kea ground-layer study data (Chun et al 2009), each representing approximately 1 minute of data, we calculated the integrated strength of the ground-layer (h<1km) and the free-atmosphere (h>1km). In addition we calculated the standard deviation of these strengths over the 30 minutes following each measurement. Each profile was then sorted by its strengths (GL and FA) and its variability. We then selected a single 30 minute sequence that had a starting profile with median/median GL and FA integrated strengths as well as median/median variability in the following half hour. These profiles were then binned into 5 minute periods and run through the PAOLA tool. The results are shown in the Figure below. The figure shows the FWHM measured on a single centrally located point. As was shown previously, the FWHM is very uniform across the field so we expect that this central point provides a reasonable measure of the variations.

The absolute variations are about a factor of two larger than the seeing-limited variations. These plots should be taken as a starting illustration of the variation of the FWHM with time. A central limitation on this analysis is that it is not known how the profile very close to the pupil of CFHT is distributed nor how it varies with time.

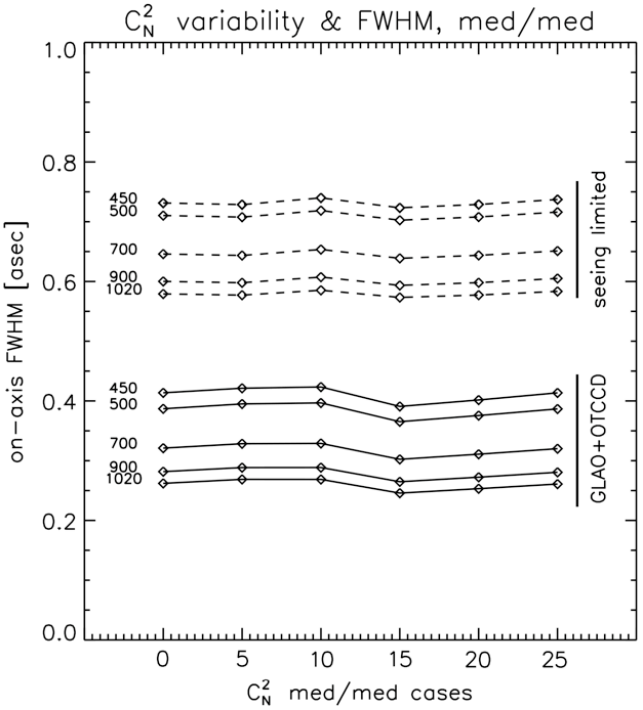

Figure 34: Example variability of the GLAO+OTCCD FWHM over a 30 minute period showing typical GL and FA strengths and variability.

5.6.7 What is the shape of the PSF?

The `IMAKA PSF is dominated by the residual free-atmosphere seeing and as such we expect the PSF will be more like a typical seeing-limited image than the canonical PSF of a classical AO system. Indeed, at the bluer wavelengths the shape is well described by a Moffat profile (Figure below). At the redder wavelengths the residual wavefront aberrations are small enough that the PSF deviates from this shape and we begin to see a halo and core to the PSF. The figure below shows a cut of the average PSF within the one-degree diameter field of view of `IMAKA for the COSMOS simulations. Only the wavelengths 0.5, 0.7, and 0.9 microns are shown. Each average PSF is fit with a Gaussian, Lorentzian, and Moffat profile. The Gaussian and Lorentzian profiles are never good fits. The Moffat profile is a good fit for the bluer wavelengths (namely where the phase variance is still large) but starts to deviate from the PSF at the longer wavelengths.

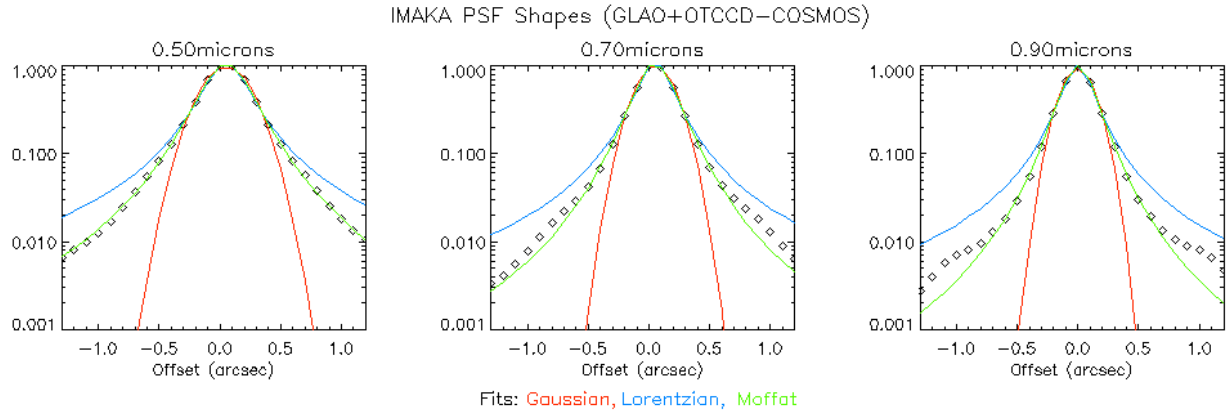

Figure 35: The shape of `IMAKA PSFs. A cut across the average PSF (symbols) is shown for wavelengths of 0.5, 0.7, and 0.9 microns. Three models are fit to the data (gaussian (red), Lorentzian (blue), and a Moffat (green) profile. The PSFs shown here are from the GL-median, FA-median COSMOS simulations.

5.7 Improvements to the performance simulations

From a purely AO point of view, `IMAKA does not push the technological or performance

boundaries. We believe we have addressed within this study the feasibility of the concept. Although the concept is understood, it's implementation here is innovative and there are subtle issues that need to be kept in mind as the instrumental concept matures. Some of these issues are due to lack of sufficient data, others due to lack of time to explore them in detail, but they will need to be answered in any further studies.

- *$C_N^2(h)dh$ profile*: To this point we have used the Ground layer profile that was measured from the roof of the UH 88" telescope. This had just enough resolution (dh~15m) to discern two thin layers near the ground. The OTP experiment has provided some statistics of the relative occurrence of dome, ground layer and free atmosphere seeing, but without probing their vertical extent. More statistics and confirmation of the conclusion of the MKGL study are needed to validate the entire concept. The path to achieve this is to be able to sense the turbulence at higher resolution through the telescope and dome itself. This is the goal of the OTPv2 experiment. The very high vertical resolution profiles can be fed to the simulations to improve the realistic performance of GLAO, although we do not expect large differences in performance.

- *Missing error terms in GLAO budget*: The current error budget accounts for the largest, dominant error terms. A detailed error budget will need to include error terms associated with wavefront sensing, temporal lag (which we can obtain from PAOLA), and reconstruction error. While these terms are all small when compared to the free atmosphere seeing and residual error, care has to be taken that they do not add excessively. Finally, there are some error terms related to real world implementation that cannot easily be simulated *ab initio*, but can be included as they arise to constantly monitor the expected performance during development. These might include aberrations introduced by optical elements, alignment errors, or what kind of dome seeing to expect after the dome will have been vented.

- *OTCCD performance:* The performance of OTCCD arrays is still subject to debate especially in an operational context. We have currently implemented a simple model of nearest neighbor measurement and integer pixel correction; we also neglect the bandwidth error which might be large for high altitude Taylor flows and 100Hz sampling rate. Fortunately, we can keep abreast of the real world developments of OTCCD through the developments of PanSTARRS1 and ODI. Another area of concern regarding the simulations is the actual strength and distribution of the free-atmosphere turbulence: to prevent wrap-around, the altitude of the highest phase screen is set to 3000m, which is enough for GLAO purposes (the guide star beams are completely decorrelated above 300m) , although it is more likely concentrated between 6000 to 9000m above the telescope. This means that the isokinetic angle may in fact be smaller than currently expected from our simulations. The MKAM MASS/DIMM will provide statistically valuable data as input to the model.

- *Zenith/thickness of GL dependence*. So far all the simulations assume that the thickness of the optical turbulence is the same as the vertical profile; this implies that they are valid at zenith. When pointing over at a zenith angle α, the effective thickness of the layer is multiplied by a factor $1/\cos\alpha$. While `IMAKA is conceived as a near zenith instrument anyway due to the zenith angle dependence of r_0 , the effect of observing 30˚ from zenith will be to effectively reduce the size of the GLAO corrected field by a factor 1.15 in the

linear gray zone approximation. This effect needs to be simulated in greater detail to understand the limits of GLAO off-zenith.

6. Next steps and "technical" schedule

`IMAKA represents a truly unique ground-based capability for CFHT. Its scientific impact and its interest to the CFHT community is clear and broad. It brings a capability complementary to planned future space facilities (JWST, JDEM, EUCLID) as well as planned ground telescopes (TMT). An expeditious development and deployment will maximize the impact of `IMAKA across all disciplines and ensure that it has several years of unchallenged capabilities.

The most challenging hurdles to `IMAKA are the detailed design, money, and politics. The first of these we can address with a Phase A study and its results are needed before either of the latter two can be fully resolved. There is thus some urgency in moving forward with the Phase A studies.

A Phase A study will encompass a complete Conceptual/Preliminary design of the system and its major subsystems. The scope of the study will be defined in the coming months and will need to be done in collaboration with the participating labs/groups. Below we discuss some of the components of the Phase A study. They are by no means exhaustive but illustrate that we can (and must) take advantage of the developed expertise within the CFH community as well as existing subsystems that can be adapted to `IMAKA.

- Systematics: The system and subsystem requirements as well as the operational concepts will be developed to guide the overall design process. A bottom-up costing and schedule are key deliverables from the Phase A. In addition, operational concepts such as the observatory impact, observational modes, and data processing will be defined. For example, both proposed optical designs involve instruments which will face significant handling issues – the prime focus instrument will need special upper end handling arrangements, while the Cassegrain instrument is large and heavy.

- Optical design: We will initially carry both optical designs forward but with the intent to down-select to a final optical design early on. These studies will, among other things, look at materials availability, mirror substrate material selection, fabrication and mounting issues and focus, collimation and alignment requirements. These in turn will then permit the development of a detailed optical error budget and realistic optical fabrication costs and schedules.

- Opto-mechanics: The trade studies will include an initial instrument mechanical design from which weight, balance and flexure estimates can be made and will permit design iterations based on optical error budget requirements and other issues. In addition key opto-mechanical subsystems such as the ADC, filter mechanisms and wavefront sensors will have preliminary designs in Phase A. Similar subsystems exist within well-developed existing instruments but their mechanical and optical details depend on choices made in the process of developing the overall instrument layout.

- GLAO-system including wavefront sensors, DM, and control electronics/software: There is considerable adaptive optics expertise in each of the CFH communities from the detailed design of subcomponents, opto-mechanics, and control software. A preliminary design will

be developed for the full GLAO system during Phase A.

- Camera: The camera system proposed leverages the Pan STARRS camera development at the University of Hawaii IfA. However, focal plane geometries, the physical layout of the instrument, camera and controller mounting needs and the means to provide camera focus and alignment will likely lead to an evolution of the camera layout. As with other systems, costs and schedules will be developed.

- Software: Phase A software efforts will include the definition and development of software and computing structures and architectures needed for DM / wavefront sensor control and camera and instrument control, the definition of engineering level software tools and structures needed for efficient data flow and post processing. Experience from the CFHTLS and the existing Exilir data pipeline will be applied.

As an overview of the schedule for `IMAKA, we present a rough 'technical' schedule below and in Figure 36. The instrument, while imposing, can be built within an overall 5-year development plan. To meet this schedule will require an increased level of resources and a firm commitment from the observatory and its community.

Activity	**Date**	**Comment**
SAC Review	2010, May	scheduled
Phase A plan development to December Board meeting	2010, July	CFHT lead
Phase A plan release for CFI	2010, Sept	Canadian CFI competition in late 2010.
SAC review	2010, Nov	
BoD funding approval of Phase A	2010, Dec	Collaborative agreement for Phase A
Phase A initiated	2011, Jan	Appoint PM, PS, (PE?)
Phase A mid-term assessment	2011, Sept	CFI will have expert panels about this time
Phase A complete for review	2012, May	
Funding decisions	2012, May-June	Multi-partner decisions
Project LoI signed, CDR funding	2012, May	
Phase B initiated	2012, June	
Critical Design Review	2013, Oct	
Construction Decision	2013, Dec	Multi-partner contract
Delivery to CFHT	2015, Oct	
Commissioning complete and shared risk observing begins	2016, July	

The immediate task at hand is a Phase A study to detail each of the subsystems and develop the system as a whole. Firm commitments from community laboratories to the Phase A effort is essential to timely instrument development and this, along with Phase A costing and schedule refinements will need to be pursued, assuming strong SAC support, in the months prior to the Board meeting in the fall. The current IMAKA team is too small to conduct a Phase A study on its own and the staff within the facility are heavily loaded in the coming year. We will need to establish commitments from groups/labs within the Canada, France, and Hawaii community.

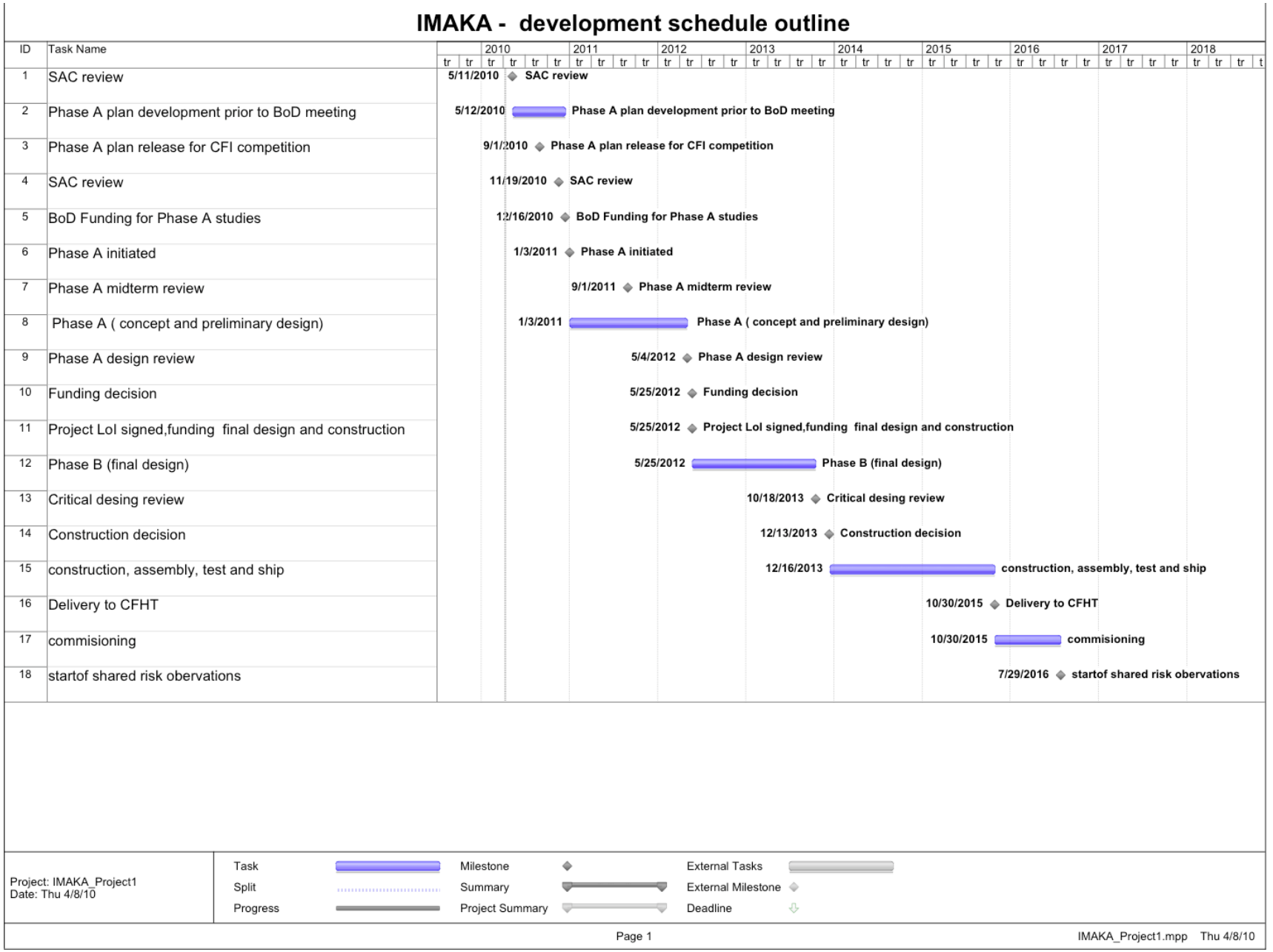

Figure 36: `IMAKA development schedule outline

6.1 Schedule Risks

The current schedule credibly overlaps the early days of JWST and will beat the 30-40m telescopes to the sky. Although aggressive, the schedule puts CFHT in a strong position to generate unequalled science at a particularly opportune time. There are however clear schedule risks which could challenge our ability to take advantage of these opportunities.

The primary schedule risks, assuming the project is supported by SAC and the Board, are the timing of the release of funds (and by implication the timing of the expansion of the CFHT partnership), timely partnering with development labs capable of providing the Phase A and Phase B engineering efforts, and delays associated with the delivery of long-lead-time items..

The most pressing need at this point is the funding of Phase A studies and the identification of labs that have the necessary technical resources and experienced manpower to undertake the Phase A studies in an expeditious manner. At a minimum this is likely to require a full time mechanical engineer and designer, an optical designer, an electronics engineer and detector specialist, two software engineers and a full time project manager. Some of these services can be obtained commercially, but at additional financial cost to the project. It should also be possible to divide the Phase A efforts between a few independent labs, although this will of necessity increase to load on the project manager. If SAC supports the project, one of the first orders of business of the current project team will be to secure letters of interest from potential providers. Costs are likely to be on the order of $1M, mostly for staffing (~8 FTE for one year), models, prototypes, and external consultants to arrive at a preliminary design ready for the Phase B final design process. However, collaborative agreements with national labs could substantially reduce this number. The period during the Phase A study will provide the opportunity to establish funding for the Phase B design and fabrication.

Mis-timing with funding opportunities is a further risk. For example, the Canadian Foundation for Innovation is expected to have a call for proposals later this year, for which we should be prepared. This will involve the identification of both a sponsoring institution and commercial partners by late summer. CFHT will need to clearly express its support for `IMAKA to take advantage of this and other opportunities

Delivery of high-lead-time components such as the large mirrors and lens blanks, the DM(s) and the detectors could be a schedule risk if not managed carefully. A strong Phase A study and timely decisions on Phase B funding could permit some of these to be ordered prior to completion of the final design and the critical design review (CDR) to offset this risk. Likewise, breakage of a major optical component late in the development cycle is a risk that can be somewhat mitigated by, for example, working with blank sizes and materials that do not involve extended delivery times.

The generation and testing of large precision aspheric surfaces is a slow process and could lead to unacceptable delays. Likewise the need to refigure the CFHT secondary mirror in the case of the Cassegrain design involves not only schedule risk due to the work involved, but risk at the level of obtaining agreement among the partners that this is a path the observatory wishes to take.

Finally there is the overall risk of small delays at various stages summing to a larger delay in the project overall. Dedication of an experienced, full project manager involved from the start of Phase A studies and vested with the authority to make decisions will go a long way toward mitigating

these risks. Similarly, collocation of as many of the principals as possible, at least for major subsystems, will greatly enhance real-time problem solving and decision making.

6.2 Technical Risk

Technical risk include the availability of components, the ability to figure and mount the large off-axis elements for the prime focus design, the ability to procure the large lens blanks for the Cassegrain design and the overall weight of the Cassegrain design.

Although, due largely to initiatives for space-based instruments and ELTs, the fabrication of large high-quality off-axis higher-order aspheric optical elements is not the daunting task of 20 years ago, it is still far from being a simple or straightforward task. Issues arising from mirror substrates selection, optical figure generation, testing and stress-free mounting are each important risk factors.

The quality of the delivered optics will only be as good as the test methods used. Modern precision testing depends to a large extent on precision profilometers and computer-generated holograms (CGHs) used in conjunction with production-line interferometers. Although the generation of CGHs is now a well-established process, their use requires highly accurate and reproducible test bench setups with geometries held to the level of 10s of microns throughout the test-polish-test final fabrication process. To mitigate these risks, care will be needed in the selection of the optical fabricator, likely one of the major optical houses, to ensure that the necessary experience and metrology are at hand and that its production schedule meshes well with the project development timeline.

Testing of large precision mirrors is ideally carried out with the mirror mounted to the support structure to be used in the instrument. Given that in-fabrication optical tests will be carried out at temperatures that are relatively warm compared to those in operation, some means of testing the final optical figure at cold temperatures should be considered to avoid last minute surprises. These issues imply that the optic support geometries should be carefully worked out fairly early in the design process, and ideally would be part of the deliverable from the optics house. It is worth noting here that, except for the DM itself, the remaining optics are not generally close to pupil image so their residual figure errors will not be corrected by the DM. This is a difference between a GLAO system and a classical AO system.

Although deformation of optical surfaces due to non-ideal mounting schemes is an age-old issue, it still plagues many otherwise well conceived instruments. Input from an experienced opto-mechanical designer will help considerably in avoiding these troublesome issues that often aren't fully appreciated until the instrument is put into service. In particular, finite element analysis can fail to sufficiently account for the effects of difficult-to-predict real-world effects such as temperature gradients across the support structure, mechanical stiction in joints, etc. This is a place where an experienced designer can make a vital contribution.

The choice of the substrate for the large mirrors will need careful consideration. Although single point diamond turned optics have many advantages in the infrared, it is not clear that they are appropriate for work at visible wavelengths. Issue of micro roughness, thermal stability, bimetallic stress and internal stress relief and annealing are all concerns Glass substrates are the most obvious choice. However, should light-weighting be needed to control total instrument weight, issues of substructure print through to the optical surface will need careful consideration. Although all of

these are potential risk, they have all been solved in one way or anther in existing instruments.

The very large lenses of the Cassegrain design are at the limit of available blank sizes, although initial inquiries by the designer indicate that they should be available. Index uniformity and deformation arising from self-weight deflections under changing gravity loads will need to be careful consideration but should be tractable.

Stray light suppression and baffling design will need to be carefully considered during Phase A studies, especially for the prime focus design where it will be particularly important to ensure that the detector sees only the beam as it leaves each of the upstream optical surfaces. Otherwise, light from the moonlit sky and nearby bright stars could lead to unacceptable background levels and focal plane artifacts. Both designs offer potential baffle locations.

The development of mildly concave and convex DMs is currently being undertaken to address the needs of several ELT instruments. One leading manufacturer, CILAS, has indicated that the mirrors needed for the designs considered for IMAKA will be within their capabilities, and will provide ROM costs and development schedules in time for the May, 2010 SAC meeting.

The development of wavefront sensors is a well understood technology that poses little technical risk. However the number of sensors, the need for field exploration, packaging around the focal surface, and minimization of field vignetting while accessing in-field reference stars are all important details which will need careful consideration during early Phase A instrument layout.

CCD procurement, camera and controller development, and flexibility in camera controller mounting are all issues that the PanSTARRS project have worked through successfully with few issues remaining at this point, so there appears little technical risk for these subsystems at this point other than perhaps time-to-develop issues.

The same goes for the generation of the AO control software and data pipeline, each of which have been developed for other instruments by the CFHT communities and for which there is a rich tradition of user community cooperation and support.

The instrument housing and thermal control, and handling and storage of the instruments off the telescope are issues that will need attention, but at this point appear to be tractable .

As a final note, many of these issues have been explored and reported in the COM DEV optical design report. This report can be made available from CFHT if desired.

6.3 Financial Risk

The main financial risks to IMAKA are the schedule-related uncertainties in the instrument funding profile discussed above and the overall instrument cost. A major component of the Phase A study will be to establish credible costs and schedules for IMAKA's development which are difficult to assess at this point. Our working point so far has been a total cost of around $12M US, but this number has little foundation other than the estimated total costs related to instruments of similar size and complexity.

Other financial risks involve potential breakage of the larger optical components and the DM, particularly if this were to occur late in their development, or failure of a manufacturer to deliver an optic of the required quality. Apart from the cost of replacing the optical blanks, such events would produce sizable schedule delays and the attendant costs for manpower incurred by prolonging the project. The effects of a broken optic however can be mitigated to some degree by choosing a design for which replacement substrates can most readily be obtained. Although not unknown, breakage is not a common issue at major optical houses and should not weigh too heavily on schedule concerns.

Other financial risks would arise from development delays of a more general nature and should be addressed in the Phase A report. Similarly, errors in the estimated subsystem development costs coming out of Phase A could be a problem unless they are well founded.